

Learning virulence-transmission relationships using causal inference

Sudam Surasinghe^{1,2}✉ and C. Brandon Ogbunugafor^{1,2,3}✉

¹Department of Ecology & Evolutionary Biology, Yale University, New Haven, CT 06520, USA

²Public Health Modeling Unit, Yale School of Public Health, New Haven, CT 06510, USA

³Santa Fe Institute, Santa Fe, NM 87501, USA

✉S.S.: sudam.surasinghe@yale.edu; C.B.O: brandon.ogbunu@yale.edu

Abstract |

The relationship between traits that influence pathogen virulence and transmission is part of the central canon of the evolution and ecology of infectious disease. However, identifying directional and mechanistic relationships among traits remains a key challenge in various subfields of biology, as models often assume static, fixed links between characteristics. Here, we introduce *learning evolutionary trait relationships* (LETR), a data-driven framework that applies Granger-causality principles to determine which traits drive others and how these relationships change over time. LETR integrates causal discovery with generative mapping and transfer-operator analysis to link short-term predictability with long-term trait distributions. Using a synthetic myxomatosis virus-host data set, we show that LETR reliably recovers known directional influences, such as virulence driving transmission. Applying the framework to global pandemic (SARS-CoV-2) data, we find that past virulence improves future transmission prediction, while the reverse effect is weak. Invariant-density estimates reveal a long-term trend toward low virulence and transmission, with bimodality in virulence suggesting ecological influences or host heterogeneity. In summary, this study provides a blueprint for learning the relationship between how harmful a pathogen is and how well it spreads, which is highly idiosyncratic and context-dependent. This finding undermines simplistic models and encourages the development of new theory for the constraints underlying pathogen evolution. Further, by uniting causal inference with dynamical modeling, the LETR framework offers a general approach for uncovering mechanistic trait linkages in complex biological systems of various kinds.

1 Introduction

Since the early 1980s, the virulence transmission tradeoff hypothesis has provided a foundational framework in the evolution and ecology of infectious diseases. It proposes that virulence (“the harm a pathogen does to its host”) [1] evolves in relation to transmission up to an optimal threshold, beyond which elevated host mortality undermines transmission, and consequently, pathogen fitness [2, 3, 4, 5, 6]. Despite its conceptual and pedagogical appeal, empirical studies reveal that this relationship is deeply *context-dependent*: correlations observed under one set of host-parasite conditions often do not hold under others [7, 8, 9, 10]. This dubiousness has encouraged the field to reflect on the assumptions underlying the relationship between virulence and transmission. That is, epidemic behaviors perceived as the product of evolutionary forces could instead be ecological or behavioral in nature [11, 12]. The idiosyncratic nature of the relationship between virulence and transmission underscores the greater need for methods that can better capture the mechanistic relationship between biological traits. Specifically, the limitations of univariate tradeoff analysis highlight the need for multivariate causal methodologies that transcend the study of disease, and can be applied across many subfields of evolutionary biology and ecology.

Causal drivers of quantitative traits are central yet often ambiguously treated in genetics, particularly for complex traits [13, 14]. Existing approaches mostly address static causality within Pearl’s [15] framework, while explicit causal studies remain scarce [16, 17, 18]. Time-series perspectives inspired by Granger’s predictive causality [19, 20] offer dynamic alternatives but are rarely applied to evolutionary scenarios [21, 22]. In epidemiology, causal modeling has advanced toward the integration of environmental, social, and biological determinants [23, 24, 25, 26, 27]. Studies often adopt Rubin’s potential outcomes framework to estimate intervention effects

[28, 29, 30], while extensions such as marginal structural models address time-varying exposures [31, 32, 33]. Recognizing that environmental drivers vary through time, time-series causal discovery is particularly valuable in the study of ecological systems. Methods such as convergent cross-mapping and related data-driven causal tools have been used to detect driver response relationships in ecosystem time series [34, 35]. In parallel, Granger-style analyses have been applied to infer environmental and behavioral drivers of incidence [36, 37, 38, 39, 40], highlighting the complementarity between predictive and interventionist causal frameworks.

Despite these advances, there remains a methodological gap in identifying causal relationships between dynamic biological traits. Such tools are essential for clarifying the elusive connection between virulence and transmission and, more broadly, for uncovering causal structure in biological systems. To address this, we introduce the *learning evolutionary trait relationships* (LETR) framework, which combines predictive causality in the Granger tradition with discrete dynamical systems. LETR employs modern information-theoretic extensions—such as transfer entropy, causation entropy, and geometric information flow [41, 42, 43]—to capture nonlinear and context-dependent interactions among traits associated with virulence and transmission in this setting. Evolutionary updates are represented as discrete generational maps, which naturally accommodate fixed points, bifurcations, and chaotic behavior [44, 45]. Using mechanistic examples, such as the myxomatosis model of Dwyer et al. [46], LETR can illustrate how virulence can act as a causal driver of transmission through within-host effects on parasite load.

We offer several original contributions. Methodologically, we present a scalable, data-driven pipeline that identifies Granger-style directional drivers from multivariate time series, fits generative update maps conditioned on those drivers, and analyzes the corresponding transfer operator to recover long-term trait distributions. The LETR framework therefore enables tests of which measured traits act as upstream causal drivers and yields population-level distributions that link mechanistic hypotheses about traits and ecological processes to empirically observable patterns. With regard to the canon in the evolution and ecology of infectious diseases, we demonstrate that static tradeoff models are insufficient for properly deconstructing the relationships between pathogen traits. Alternatively, the field should consider new theoretical models that incorporate the dynamism and context-dependence of trait relationships governing pathogen evolution.

By introducing LETR, we bridge the gap between empirical time series and theoretical models of trait correlation, providing a quantitative language for disentangling directionality and feedback in evolutionary and ecological dynamics. In doing so, we advance a broader agenda that transcends disease and applies across evolutionary biology and ecology: to move beyond static models of trait correlation, and toward a dynamic understanding of how causal linkages among traits determine long-term ecological equilibria, evolutionary trajectories, and the predictability of complex biological systems.

2 Methods

In this study, we propose a data-driven toolkit for learning trait dynamics from longitudinal observations. Here, “learning” refers to the process of inferring underlying patterns and causal relationships from data, as commonly used in machine learning and data-driven analysis, rather than traditional cognitive conceptions of learning. Modern monitoring and aggregation efforts are steadily increasing the temporal resolution and trait coverage available to epidemiologists and disease ecologists, enabling inference that moves beyond simple summary statistics and fixed distributional assumptions. The *learning evolutionary trait relationships* (LETR) framework exploits these richer time series to identify which measured traits functionally drive others and to condition on discovered drivers when fitting generative update maps. In practice, LETR is a two-stage, data-driven pipeline (see Figure 1). First, we identify Granger-predictive drivers by testing whether candidate variables improve one-step forecasts of a focal trait using geometric information flow (GeoC) [43] or alternative Granger-style measures such as transfer entropy [41] or causation entropy [42]. Second, we fit a conditional generative update map of the form $\mu_{n+1} = f(\mu_n, y_{i_n})$, using interpretable learners or regularized supervised methods, and then analyze ensemble evolution under f by approximating the Frobenius-Perron transfer operator to obtain invariant densities and long-term trait distributions [47].

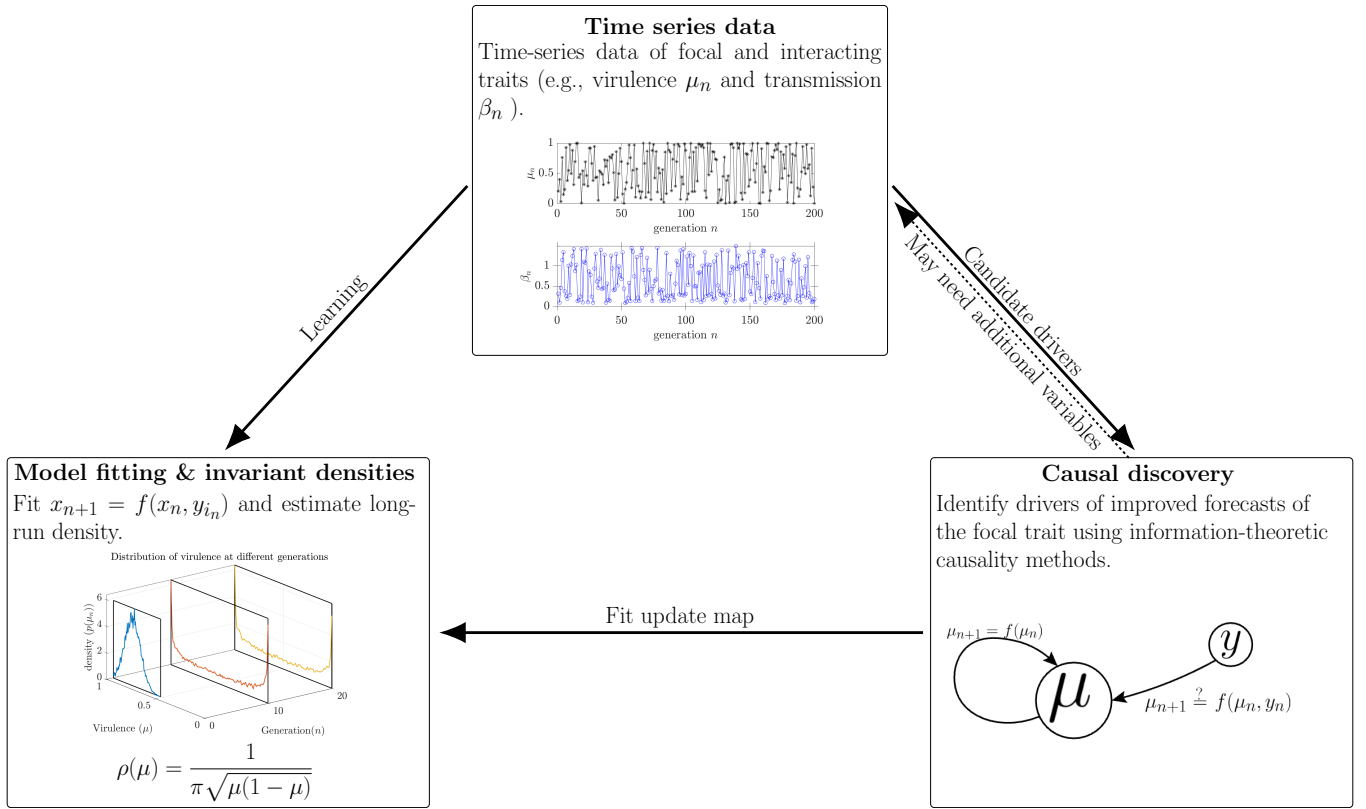


Fig. 1. Illustration of the *learning evolutionary trait relationships* (LETR) framework. The top box shows time series of focal and interacting traits, such as virulence (μ_n) and transmission (β_n), collected from evolving pathogen populations or from host-level surveillance. **Causal discovery** identifies which measured variables improve short-term forecasts of a chosen focal trait by testing whether adding a candidate predictor, such as an environmental covariate, a demographic or behavioral variable, a genetic marker, or a treatment exposure improves one-step forecasts. Methods include geometric information flow (GeoC) [43], transfer entropy [41] and causation entropy [42]. **Model fitting** fits a generative update map $x_{n+1} = f(x_n, y_{i_n})$ conditioned on drivers discovered in step one, where f may be a pedagogical map such as the logistic map or a regularized supervised learner chosen by cross-validation, and where fitted models yield interpretable summaries and partial dependence visualizations for applied researchers. **Invariant densities** analyze ensemble behavior under f by approximating the Frobenius-Perron transfer operator and estimating the invariant density of x , which summarizes the long-run distribution of the focal trait under the inferred dynamics and observed driver processes, highlights prevalent phenotypes and multimodality, and indicates how interventions may reshape stable outcomes. Arrows indicate the workflow and feedback, with dashed links from causal discovery back to the data denoting the possibility of adding additional variables to improve inference, and arrows from data to model fitting denoting direct learning of long-term behaviour from observed trajectories.

2.1 Identify Granger causal variables

We are interested in identifying the causal variables associated with the trait of interest. In this study, we focus on virulence, denoted as μ , as the trait of interest. However, readers may substitute virulence with any trait relevant to their study.

The virulence data may not be fully explained by its previous generation value. Therefore, we are interested in understanding the potential influence of other Granger causal variables on virulence. Granger causality explores whether one time series can predict the behavior of another time series (see Supporting Information Figure S1). In other words, we are interested in exploring the following question: “Is an additional variable y required to elucidate the relationship between the present and past data of a variable x (in this case, virulence)?”

This question involves distinguishing between two alternative versions of the potential origins of μ_{n+1} and is based on choosing one of the following two cases:

$$\mu_{n+1} = f(\mu_n), \quad \text{or} \quad \mu_{n+1} = f(\mu_n, y_n), \quad (1)$$

to describe the actual function f . We use the shorthand notation:

$$\mu_{n+1} \triangleq f(\mu_n, y_n) \quad (2)$$

to represent the above statement. We also employ a geometric measure for causality, $GeoC(\cdot)$ [43], to determine the conditional information flow, as measured by the difference in the correlation dimension of the data sets $[\mu_n, \mu_{n+1}]$ and μ_n :

$$GeoC(\mu_{n+1} | \mu_n) = D_2([\mu_n, \mu_{n+1}]) - D_2(\mu_n), \quad (3)$$

where $D_2(\cdot)$ represents the correlation dimension of the given set. The geometric measure for causal inference from y to μ can therefore be computed as

$$GeoC_{y \rightarrow \mu} = GeoC(\mu_{n+1} | \mu_n) - GeoC(\mu_{n+1} | \mu_n, y). \quad (4)$$

If virulence is not influenced by any additional causal variable, then $GeoC(\mu_{n+1} | \mu_n)$ should be approximately zero, or both μ_n and $[\mu_n, \mu_{n+1}]$ reside on manifolds of the same dimension. In this case, adding any additional variable y does not change the value of the conditional geometric information, i.e., $GeoC(\mu_{n+1} | \mu_n, y)$ remains the same as $GeoC(\mu_{n+1} | \mu_n)$. Hence, $GeoC_{y \rightarrow \mu} \approx 0$ for any y in this scenario.

When $GeoC(\mu_{n+1} | \mu_n) \gg 0$, it implies the existence of at least one causal variable and highlights the necessity to update the model by identifying such a variable. In such instances, expert reasoning or prior knowledge can be employed to consider potential causal variables, which can then be added to the existing dataset by incorporating their respective time series data. Subsequently, the conditional geometric information flow of the new dataset can be analyzed to assess the effect of the considered causal variable. It is worth noting that multiple causal variables may influence virulence, and a systematic evaluation of geometric information flow could help identify them. Box 1 summarizes this process as a framework.

Box 1. Framework for learning virulence (the *trait of interest*)

1. **Data:** Utilize time series data of $N \times 1$ vector μ to construct vectors $\mu_n = \mu(1 : end - 1)$ and $\mu_{n+1} = \mu(2 : end)$.
2. Compute the correlation dimension ($D_2(\cdot)$) and assess the conditional geometric information flow: $GeoC(\mu_{n+1}|\mu_n) = D_2([\mu_n, \mu_{n+1}]) - D_2([\mu_n])$.
3. **If** $GeoC(\mu_{n+1}|\mu_n) \approx 0$:
 - There are no effective causal variables for μ ; hence, μ_{n+1} can only be modeled by μ_n .
 - Identify a discrete map f that is fitted to the data, satisfying the relationship $\mu_{n+1} = f(\mu_n)$. For instance, consider the logistic map $f_a(\mu) = a\mu(1 - \mu)$ with a parameter a .
 - Leveraging insights into the map's qualitative behavior, interpret how virulence evolves over generations. Explore whether it tends to settle into a stable fixed point, follow a periodic pattern, exhibit a chaotic trajectory, or display other dynamic behaviors.
 - Utilize transfer operators to analyze the temporal changes of population densities related to virulence.
4. **else**
 - Consider a causal variable y for μ through expert reasoning or prior knowledge.
 - Then, incorporate time series data y_n into the current dataset of μ_n .
 - Now, utilize the datasets $[\mu_{n+1}|\mu_n, y_n]$ and $[\mu_n, y_n]$ to assess the conditional geometric information flow $GeoC(\mu_{n+1}|\mu_n, y_n) = D_2([\mu_{n+1}, \mu_n, y_n]) - D_2([\mu_n, y_n])$.
 - **if** $GeoC(\mu_{n+1}|\mu_n, y_n) \approx 0$:
 - Only causal variable is y and use supervised learning methods to fit the data to the model $\mu_{n+1} = f(\mu_n, y_n)$.
 - Utilize transfer operators to analyze the temporal changes of population densities related to virulence.
 - **else**
 - Consider another causal variable z and repeat the process until all the causal variables have been identified.

2.2 Learning virulence using discrete maps and transfer operators

Virulence is a canonical idea within various subfields of infectious diseases, often defined as the harm a pathogen inflicts on its host. It can be measured in different ways across host-parasite systems, with implications for how we identify relationships between it and other traits [8, 10]. In this study, we use the host population's mortality rate attributable to the pathogen's influence (often summarized in public health as case fatality rate, CFR) as a proxy for virulence. While this definition might be very specific, the virulence literature has been famously dubious about how to measure it in host-parasite systems [8]. Consequently, to minimize ambiguity in how we define virulence, we define host death as the ultimate form of harm to a host. We hypothesize that virulence undergoes temporal variations driven by underlying changes in the pathogen's characteristics. For demonstration purposes, we utilize a simplified model of virulence that excludes additional causal variables. A numerical illustration using the logistic map, together with poliovirus mortality data, is provided in Supporting Information Section S2. The virulence of the pathogen at its n^{th} generation is denoted by μ_n , and is constrained to the unit interval. To model the dynamics of virulence, deterministic or random maps can be employed. Here, our focus lies on deterministic

maps, specifically represented by the map f operating on the unit interval $[0, 1]$:

$$\begin{aligned} f : [0, 1] &\rightarrow [0, 1], \\ \mu &\mapsto f(\mu). \end{aligned} \quad (5)$$

The qualitative behavior of these maps can be employed to model the dynamics of virulence. Evolutionary and ecological dynamics embodied in host-parasite interactions can give rise to various dynamical behaviors of virulence, such as asymptotically stable fixed points, periodic orbits, or even chaotic trajectories.

When the map f is chaotic, analysis often involves considering an ensemble of many initial conditions, rather than following a forward time orbit $\mathbb{O}^+ = \{\mu, f(\mu), f^2(\mu), \dots\}$ from a single initial condition [48]. This scenario can be analyzed using a transfer operator known as the Frobenius-Perron operator. This operator is employed to describe the orbit of ensembles when they are distributed in $p \in L^1([0, 1])$, and the map f is a nonsingular transformation and measurable relative to a Borel sigma algebra set. The Frobenius-Perron operator is a linear map, $\mathcal{P}_f : L^1([0, 1]) \rightarrow L^1([0, 1])$, which follows the discrete continuity equation,

$$\int_B p_{n+1} d\nu = \int_{f^{-1}(B)} p_n d\nu, \text{ for any } B \in \mathbb{B}, \quad (6)$$

where $\mathbb{B} \subseteq [0, 1]$ is the Borel sigma algebra of measurable sets with measure ν , and p_n denotes the n^{th} iteration of the initial density. For differentiable maps, this simplifies to:

$$\mathcal{P}_f[p](\mu) = \sum_{y: \mu=f(y)} \frac{p(y)}{|Df(y)|}, \quad (7)$$

where, if $f(y)$ is a univariate function, $|Df(y)| = |f'(y)|$ represents the absolute value of the derivative. For multivariate functions, it corresponds to the determinant of the Jacobian matrix. Additionally, the invariant density (fixed point) of the operator, expressed as π :

$$\mathcal{P}_f[\pi] = \pi, \quad (8)$$

is often of interest for understanding the long-term behavior of the variable of interest [48]. Here, we use the transfer operator to elucidate the behavior of virulence (variable of interest) when the logistic map undergoes chaotic behavior.

3 Results

In this section, we present the analyses of two case studies that provide methodological validation and empirical application for the LETR framework. Specifically, we structure the results as follows:

- **Case study I:** Method validation using synthetic data from a myxomatosis model, in which we test whether LETR recovers known directional influences inferred from the model (Section 3.1).
- **Case study II:** Applied analysis of worldwide epidemiological data on SARS-CoV-2, in which we perform Granger style causal discovery, fit conditional generative maps, and estimate invariant densities for virulence and transmission (Section 3.2).

Here, we assume that only a single strain of the pathogen enters a given host, and that the pathogen exits the host as a single strain, which may differ from the entering strain. In our analyses, we assume the transmission rate, β_n , and virulence, μ_n , to be dynamic variables. Subscripts denote the generation (or time step); for instance, β_n denotes the transmission rate of the pathogen in the n^{th} generation (or time step). We also refer readers to Supporting Information Figure S6 for a graphical illustration of these assumptions. Figure S6 illustrates the process by which a pathogen in the n^{th} generation, characterized by parameters μ_n and β_n , enters a host and undergoes mutations and ecological changes. As a result, the pathogen exits the host with updated parameters μ_{n+1} and β_{n+1} in the $(n + 1)^{\text{th}}$ generation. However, when the data lacks a clearly defined generational structure, we treat each unit of time as a single generation and denote n as the corresponding time step.

The goal is to model the dynamics of these variables, assuming that the $(n + 1)^{\text{th}}$ generation is influenced solely by the n^{th} generation values. This assumption implies that mutations and ecological factors within the current host determine the characteristics of the pathogen as it exits the host. This process was modeled using the concept of a discrete map. In classical modeling approaches, descriptive statistics are used to represent parameter values or to trace the path from a single initial condition. In this study, we examine the dynamics of ensembles of initial values for the parameters of pathogens under a discrete map that represents evolutionary and ecological changes (see supporting information Figure S7). In the results section, we present a detailed analysis of causal discovery using synthetic benchmarks (Case 1) and worldwide epidemiological data on a modern pandemic of SARS-CoV-2 (Case 2). We also provide data-driven estimates of the invariant densities of virulence and transmission for the global SARS-CoV-2 record.

3.1 Case study I: Causal model for virulence and transmission in a synthetic dataset of myxomatosis

The story of myxomatosis provided scientists with an unprecedented opportunity to observe and document the real-time co-evolution of both host and pathogen in natural populations [49, 50]. When the highly virulent myxoma virus was released into Australian rabbit populations in 1950 and European rabbit populations in 1952, it initially caused extremely high mortality rates, but less virulent strains evolved, while rabbits simultaneously evolved genetic resistance [49, 51, 52]. This system produced one of the greatest examples of rapid evolutionary change ever recorded and demonstrated that virulence evolution involves complex tradeoffs between transmissibility and host survival [53]. In light of this, we utilize it as a case study for our exploration of the utility of the LETR method.

Synthetic data motivated by myxomatosis. Dwyer et al. [46] provide the mechanistic motivation for our synthetic experiments. In their myxomatosis model the within-host virus concentration follows a Ricker form $v(t) = k_1 t e^{-k_2 t}$ and the fitted parameters k_1, k_2 are regressed on strain case mortality so that virulence maps to the timing and magnitude of within-host infectiousness [46]. Empirically, the probability that a vector acquires infection from an infected host increases with within-host viral titer. Consequently, changes in case mortality propagate through the chain $\text{CM} \mapsto (k_1, k_2) \mapsto v(t) \mapsto \text{transmission probability}$ [46, 54]. Dwyer and colleagues showed that modest shifts in host life history, seasonal forcing or resistance can move the system among equilibria, sustained cycles and period doubling, which demonstrates that virulence time series may be complex even when the underlying rules are deterministic and that past virulence can therefore carry information about future transmission. These mechanistic links motivated our synthetic design, which emulates non-Gaussian trait densities, a strongly self predictive virulence trajectory, and an asymmetric causal structure in which past virulence improves prediction of future transmission while the reverse effect is weak. To construct a controlled benchmark we simulated:

$$\begin{aligned} \mu_{n+1} &= 4\mu_n(1 - \mu_n), \\ \beta_{n+1} &= 1.5 \operatorname{sech}^2(\mu_n + \beta_n). \end{aligned} \tag{9}$$

The resulting time series are summarized in supporting information Figure S8 and in supporting information Section S2.2.3.

3.1.1 Simulated virulence and transmission dynamics

Figure 2 highlights key aspects of the diversity observed in both virulence and transmission rate within the simulated model. Using density plots, we present the distributions of these two critical parameters, emphasizing their variability and departures from conventional assumptions, such as normality. As illustrated in panel (c), the relationship between virulence and transmission rate deviates from the simplistic correlational patterns often assumed in many standard models from ecology and evolutionary biology (e.g., life history theory, the evolution of virulence) [5, 55]. This deviation underscores the need to employ more advanced analytical methods that extend beyond basic tradeoffs or associations. Consequently, it serves as a demonstrative example of how our framework can be applied to real-world experimental or observational data, offering deeper insights into invariant densities and the causal mechanisms driving dynamic processes.

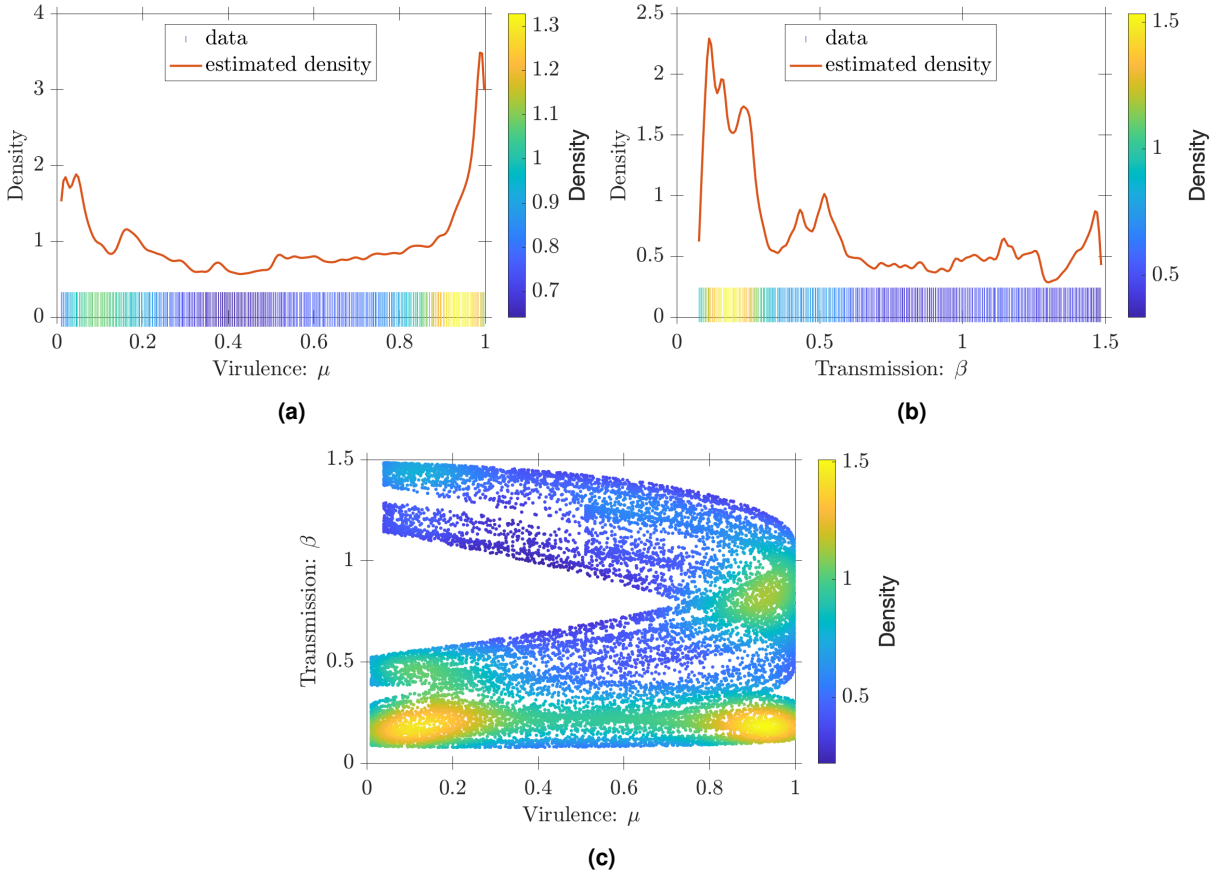


Fig. 2. Simulated complex relationship between virulence and transmission, motivated by myxomatosis. We illustrate the complex relationship between virulence and transmission trait dynamics using a methodological benchmark. (a) The marginal density of virulence μ estimated by kernel density estimation and departs markedly from a Gaussian form, exhibiting skewness and heavy tails that indicate a nontrivial probability of extreme virulence values. (b) The marginal density of transmission β is likewise skewed and not well summarized by mean and variance alone. (c) The joint density of μ and β reveals a nonlinear, non-monotonic, and complex relationship between the traits. The dataset was constructed to avoid Gaussian assumptions and a simple tradeoff structure, providing a demanding test case for causal discovery methods. The complex dynamics underscore the need for flexible, data-driven causal inference when interpreting biological trait relationships.

3.1.2 Visualizing simulated data to identify Granger causal relationships

Following the framework suggested in Box 1, we apply causal inference techniques to the generated data to identify the relationships between these variables. This process begins by visualizing the data of the n^{th} versus the $(n+1)^{\text{th}}$ generation virulence (and similarly for transmission) to assess the possibility of causal relationships (see Figure 3).

In Figure 3a, the virulence data (μ) exhibits a strong relationship between μ_n and μ_{n+1} , indicating that the dynamics of virulence can be effectively captured with a lower-dimensional model. This suggests that the relationship between μ_n and μ_{n+1} is relatively straightforward, with the data points aligning closely along a one-dimensional manifold. In contrast, Figure 3b depicts the transmission rate data (β), which does not exhibit a clear relationship between β_n and β_{n+1} . The transmission data appears to occupy a higher-dimensional space, indicating more complex dynamics that are not easily captured by its own past values alone. This lack of a clear pattern suggests that additional factors or more sophisticated modeling approaches may be necessary to fully understand the transmission dynamics, highlighting the need to incorporate causal variables into the model.

Consequently, we test virulence as a potential causal variable for the transmission rate. To visualize this relationship, we plot β_{n+1} against μ_n and β_n (see Figure 3c). The data appear to lie on a two-dimensional manifold, suggesting that the transmission rate at the $(n+1)^{\text{th}}$ generation can be fully explained by the virulence

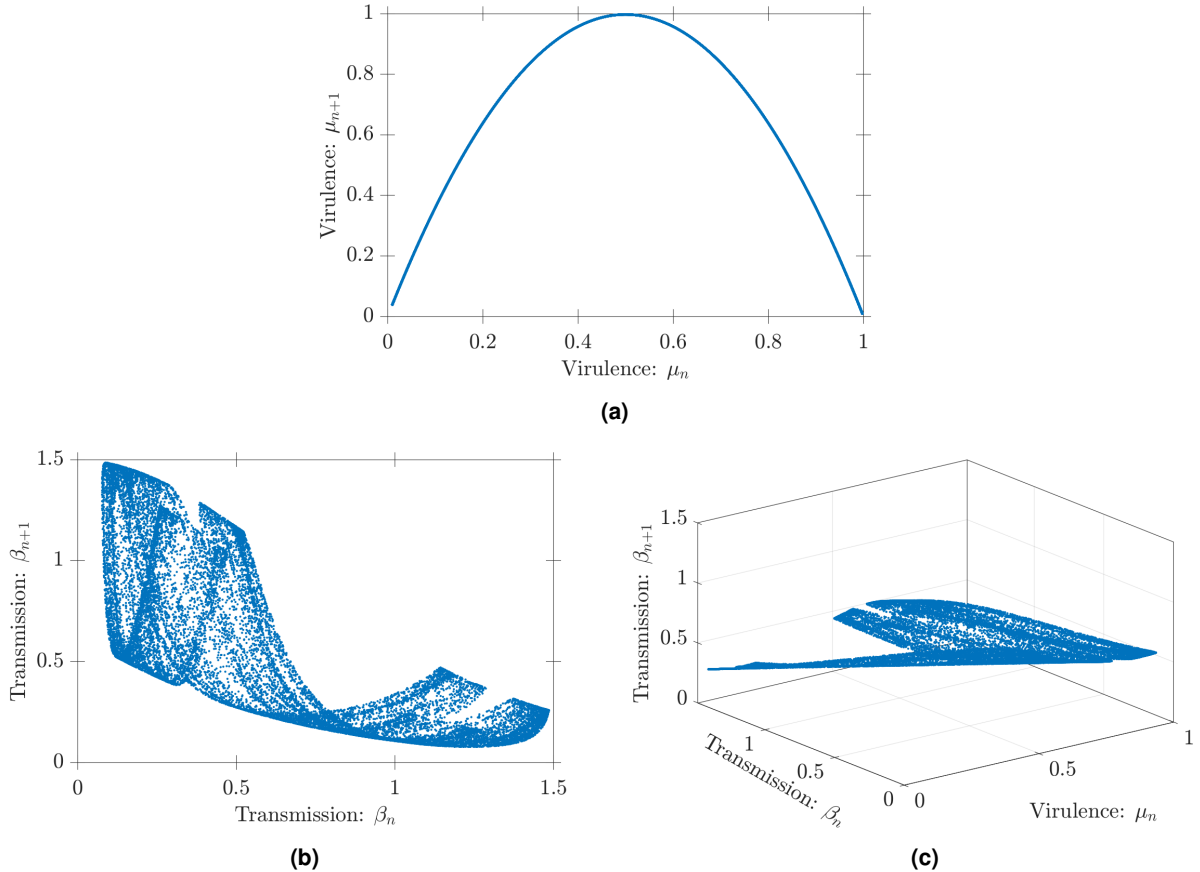


Fig. 3. Geometric diagnostics of the virulence-transmission causal model based on synthetic data inspired by myxomatosis. One-step relationships between consecutive generations illustrate that past virulence improves the prediction of future transmission. (a) Scatter plot of μ_n versus μ_{n+1} , showing a tight low-dimensional relationship consistent with strong self-predictability of virulence and the existence of a parsimonious update map for μ . (b) Scatter plot of β_n versus β_{n+1} , showing weak one-step predictability when using β alone. The point cloud lies in a higher-dimensional space than a simple one-dimensional curve. The estimated correlation dimension for the pair $[\beta_n, \beta_{n+1}]$ is approximately 1.17, indicating that β dynamics are not adequately described by a one-dimensional map in β and that additional drivers are required. (c) Scatter plot of (μ_n, β_n) versus β_{n+1} , showing that the point cloud lies on an effectively two-dimensional manifold, thereby recovering the structure absent from panel (b). Together, the contrast between panels (a) and (b) and the structural recovery in panel (c) provide visual and model-free evidence that μ_n carries predictive information for subsequent transmission. Quantitative confirmation of these observations is provided by geometric causal inference and correlation dimension estimates presented in the main text. This figure illustrates the geometric validation of the recovery of the hidden benchmark causal structure and captures the expected virulence-transmission dynamics with complex, biologically relevant trait interactions.

and transmission rate at the n^{th} generation. This observation underscores that, according to our data, virulence is a Granger causal variable for the transmission rate. A more in-depth analysis can be conducted by following the framework outlined in Box 1 to measure causal inference, thereby demonstrating the key concepts of this project.

3.1.3 Testing causal variables for virulence in synthetic data

Using the available data, we first follow the second step of the framework outlined in Box 1 to understand the causal model for the dataset. In this section, we examine the effect of virulence at a given time, based on its value from the previous time step. This approach can be used to assess whether additional variables, such as the transmission rate, are necessary to accurately predict virulence behavior. To evaluate this potential Granger causality, various causal inference methods can be employed, such as geometric causal inference, transfer

entropy, or Granger's ARMA test. In this study, we adopt geometric causal inference, which provides a more detailed analysis from a geometric perspective. Consequently, the dimensionality discussion, supported by the visual tools from the previous section (Section 3.1.2), can now be quantified using the correlation dimension, thereby aiding in the identification of causal variables.

To illustrate the flow of information, specifically the causal effect from the transmission rate (β) to the virulence (μ), we compute the correlation dimension for multiple time series datasets. The resulting values are presented in Table 1, and the geometric causal inference ($GeoC_{\beta \rightarrow \mu}$) is defined as follows:

$$GeoC_{\beta \rightarrow \mu} = GeoC(\mu_{n+1} | \mu_n) - GeoC(\mu_{n+1} | \mu_n, \beta_n) = 0.000021 \approx 0. \quad (10)$$

This result indicates that there is no discernible causal effect of the transmission rate on virulence in the given dataset.

Table 1. Correlation dimension $D_2(\cdot)$ and conditional geometric information flow $GeoC(\cdot | \cdot)$ for the virulence μ and transmission rate β datasets, used to compute the geometric causal inference from transmission rate to virulence. Correlation dimension estimates were computed using MATLAB's `correlationDimension` function [56]. Estimation procedures for geometric information flow are described in the Methods section.

Term	Value	Description/Remarks
$D_2(\mu_n)$	0.950295	
$D_2([\mu_n, \mu_{n+1}])$	0.950337	
$GeoC(\mu_{n+1} \mu_n)$	0.000042	There are no effective causal variables for μ , and μ_{n+1} can be modeled by the function $f(\mu_n)$.
$D_2([\mu_n, \beta_n])$	1.649863	
$D_2([\mu_n, \mu_{n+1}, \beta_n])$	1.649884	
$GeoC(\mu_{n+1} \mu_n, \beta_n)$	0.000021	The inclusion of β_n does not provide any additional information.

3.1.4 Testing causal variables for transmission in synthetic data

In this subsection, we focus on identifying the causal variables influencing the transmission rate, utilizing the same synthetic dataset employed in Section 3.1.3. The computed values of the correlation dimension, along with the geometric information measures, are summarized in Table 2.

Notably, while β_n lies on a one-dimensional manifold, $[\beta_n, \beta_{n+1}]$ resides on a two-dimensional manifold. Therefore, additional information is required to fully comprehend the transmission rate. In this case, we tested μ_n as the additional causal variable influencing the transmission rate. Our findings indicate that both $[\beta_n, \mu_n]$ and $[\beta_{n+1}, \beta_n, \mu_n]$ lie on two-dimensional manifolds with approximately the same correlation dimension. This leads us to conclude that virulence is a causal variable for the transmission rate in this dataset. Furthermore, we can compute the geometric causal inference of virulence on the transmission rate, as demonstrated in the following equation.

$$GeoC_{\mu \rightarrow \beta} = GeoC(\beta_{n+1} | \beta_n) - GeoC(\beta_{n+1} | \mu_n, \beta_n) = 0.673872. \quad (11)$$

To summarize the overall causal inference discussed in Section 3.1, we illustrate the causal model of virulence and transmission rate based on the synthetic data in supporting information Figure S9, highlighting the key relationships among the variables.

Table 2. Correlation dimension $D_2(\cdot)$ and conditional geometric information flow $GeoC(\cdot|\cdot)$ for the virulence μ and transmission rate β datasets, used to compute the geometric causal inference from virulence to transmission rate. Correlation dimension estimates were computed using MATLAB’s `correlationDimension` function [56].

Term	Value	Description/Remarks
$D_2(\beta_n)$	0.986140	Reside on a one-dimensional manifold.
$D_2([\beta_n, \beta_{n+1}])$	1.660012	
$GeoC(\beta_{n+1} \beta_n)$	0.6739	There is an effective causal variable for β , and β_{n+1} cannot be modeled solely by β_n .
$D_2([\beta_n, \mu_n])$	1.649863	Reside on a two-dimensional manifold.
$D_2([\beta_n, \beta_{n+1}, \mu_n])$	1.649891	Reside on a two-dimensional manifold.
$GeoC(\beta_{n+1} \beta_n, \mu_n)$	0.000028	β_{n+1} can be modeled as a function of β_n and μ_n .

3.2 Case study II: LETR analysis of causality and invariant distributions in a modern pandemic dataset

In the previous example, we highlight the relevance of our approach by using simulated and synthetic data sets that model real-world phenomena. Next, we analyze the transmission and virulence dynamics of a modern pandemic, SARS-CoV-2, using real-time data.

Global pandemic dataset. For modern pandemic analyses, we use the daily time series of global SARS-CoV-2 case incidence and case fatality rates, obtained from Our World in Data. The dataset covers the period from 1 September 2020 to 24 August 2025. We use the case fatality rate (CFR) [57] as a proxy for virulence μ and daily new cases per million people [58] as a proxy for transmission. To prevent feature dominance and improve model performance [59], we rescale the transmission series to the unit interval $[0, 1]$ using min-max normalization (each data point x is rescaled as $\frac{x - \min x}{\max x - \min x}$) and denote the scaled values by β . These measures are coarse proxies that do not necessarily capture within-host virulence or the instantaneous transmission rate. Any alternative proxy that better represents the underlying trait may be substituted into the LETR framework. In this study, we use these proxies to illustrate the practical application of LETR. The primary objective is to assess the plausibility of Granger-style causal drivers for each trait and to test whether one trait exerts a causal influence on the other.

To illustrate the underlying dynamics and the relationship between virulence and transmission, we plot the phase space of virulence versus transmission in Figure 4a and the corresponding time series in supporting information Figure S1. The scatter plot in Figure 4a reveals a nonlinear association broadly consistent with a virulence transmission tradeoff and well approximated by an L-shaped inverse curve. Using the MATLAB nonlinear regression function `nlinfit`, we fit a simple reciprocal model to the data and obtained $\beta \approx 0.228/\mu$, as shown in Figure 4a. In this pattern, transmission is high at very low virulence, declines rapidly as virulence increases slightly, and remains low at higher virulence values. At the lower end of the virulence range, the point cloud is highly scattered around the fitted curve. This dispersion may reflect heterogeneity in behavioral, social, and public health responses when measured virulence is low, together with reporting and detection biases that are more influential in that regime.

3.2.1 Causal discovery of virulence–transmission dynamics in SARS-CoV-2

Geometric information flow can be used to identify plausible Granger-style causal drivers of virulence and transmission from their respective time series. In particular, visualization of pairwise time series in scatter plots aids the assessment of these causal hypotheses by revealing low-dimensional structure and predictive geometry that indicate whether one variable carries information about the future of another. Figure 4 illustrates these scatter plots. Figure 4b shows the one-step relationship μ_n versus μ_{n+1} for virulence and Figure 4c shows the one-step

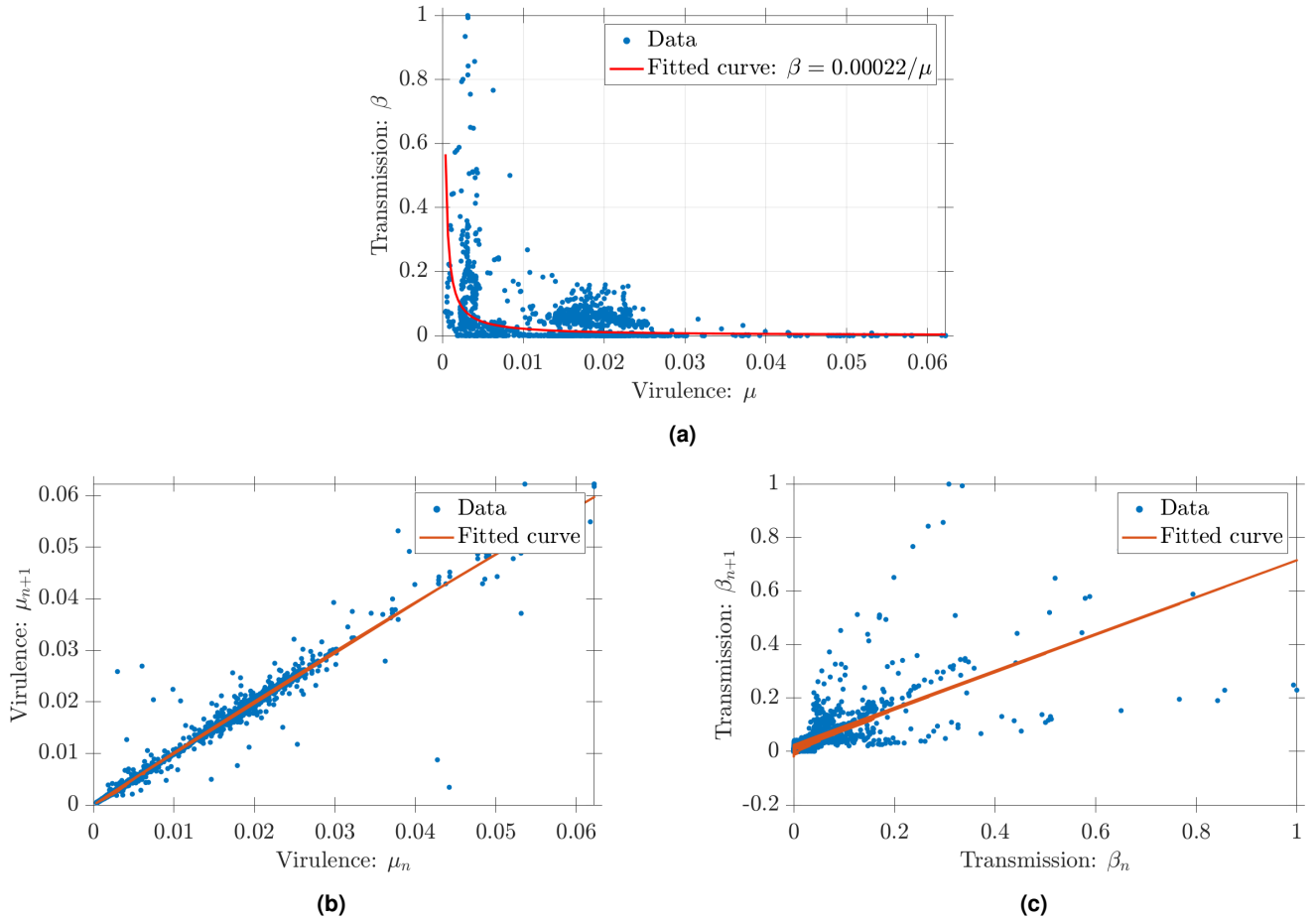


Fig. 4. Geometric investigation of SARS-CoV-2 trait dynamics. One-step relationships show that virulence is largely self-predictive while transmission is more dispersed and likely requires additional causal predictors. Data points are daily observations from Our World in Data [57, 58] for the period 1 September, 2020 to 24 August, 2025. (a) The phase space μ versus β with a reciprocal fit $\beta \approx 0.228/\mu$ obtained by nonlinear regression. (b) shows μ_n versus μ_{n+1} and reveals a tight one-dimensional manifold consistent with strong temporal predictability of virulence. (c) shows β_n versus β_{n+1} , which exhibits substantially greater dispersion and a structured pattern in which higher transmission values separate into three apparent branches, suggesting more complex dynamics and the plausibility of additional causal drivers. Together, these patterns geometrically illustrate the asymmetric causal structure between virulence and transmission and indicate that predicting transmission may require additional ecological, social, or behavioral variables beyond virulence alone.

relationship β_n versus β_{n+1} for transmission. These data indicate that virulence, shown in Figure 4b, is tightly clustered around a clear one-dimensional curve. Therefore, most predictive information on the next time step appears to be contained in the current value of virulence alone. The minor scatter around the curve may reflect observational noise, such as reporting errors or the influence of weak additional drivers. By contrast, the transmission scatter plot in Figure 4c exhibits substantially greater dispersion, although it also shows structure with higher transmission values that separate into three apparent branches. This pattern implies more complex transmission dynamics and suggests the plausibility of additional causal drivers. Therefore, we apply the geometric information flow measure to quantify these hypotheses and to test whether virulence and transmission exert causal effects on one another.

Table 3 reports correlation dimension estimates and conditional geometric information flow measures for the SARS-CoV-2 virulence and transmission time series. The correlation dimension of virulence alone, $D_2(\mu_n) \approx 0.96$, is close to $D_2([\mu_n, \mu_{n+1}]) \approx 1.07$. Together with $\text{GeoC}(\mu_{n+1} \mid \mu_n) \approx 0.112$, these values indicate that most short-term predictability of μ_{n+1} is contained in μ_n . Including β_n provides only marginal additional information, with $\text{GeoC}(\mu_{n+1} \mid \mu_n, \beta_n) \approx 0.099$ and a small net effect $\text{GeoC}_{\beta \rightarrow \mu} \approx 0.013$. This pattern suggests that transmission is, at best, a weak causal predictor of subsequent virulence. By contrast, transmission exhibits a different

Table 3. Geometric information measures for virulence μ and transmission β time series for SARS-CoV-2. $D_2(\cdot)$ denotes the correlation dimension, and $GeoC(\cdot | \cdot)$ denotes the conditional geometric information flow. Correlation dimension estimates were computed using MATLAB’s `correlationDimension` function [56]. Geometric information measures indicate that transmission exerts a weak causal influence on virulence, whereas virulence exerts a relatively stronger causal influence on transmission.

Term	Value	Description/Remarks
$D_2(\mu_n)$	0.960042	
$D_2([\mu_n, \mu_{n+1}])$	1.072071	
$GeoC(\mu_{n+1} \mu_n)$	0.112029	Low value and scatter plot (Figure 4b) imply most predictive information for μ_{n+1} resides in μ_n , so μ_{n+1} can be modeled as $f(\mu_n)$. Minor deviations may reflect weak causal influences or observational noise.
$D_2([\mu_n, \beta_n])$	1.271778	
$D_2([\mu_n, \mu_{n+1}, \beta_n])$	1.371026	
$GeoC(\mu_{n+1} \mu_n, \beta_n)$	0.099248	Including β_n provides only marginal additional predictive information beyond μ_n .
$GeoC_{\beta \rightarrow \mu} = GeoC(\mu_{n+1} \mu_n) - GeoC(\mu_{n+1} \mu_n, \beta_n) = 0.012781$		
$D_2(\beta_n)$	0.693734	
$D_2([\beta_n, \beta_{n+1}])$	1.001665	
$GeoC(\beta_{n+1} \beta_n)$	0.307931	There may be an effective causal variable for β , and β_{n+1} may not be modeled solely by β_n .
$D_2([\beta_n, \mu_n])$	1.271778	
$D_2([\beta_n, \beta_{n+1}, \mu_n])$	1.309606	
$GeoC(\beta_{n+1} \beta_n, \mu_n)$	0.037828	Virulence shows a detectable causal influence on transmission, but additional variables may be required to fully account for transmission dynamics.
$GeoC_{\mu \rightarrow \beta} = GeoC(\beta_{n+1} \beta_n) - GeoC(\beta_{n+1} \mu_n, \beta_n) = 0.270103$		

profile. The one-step predictability of β from its own past, $GeoC(\beta_{n+1} | \beta_n) \approx 0.308$, suggests that additional co-variates are needed to model transmission dynamics. When μ_n is incorporated, the conditional measure falls to $GeoC(\beta_{n+1} | \beta_n, \mu_n) \approx 0.038$, yielding a net contribution $GeoC_{\mu \rightarrow \beta} \approx 0.270$. This result indicates that virulence supplies substantial complementary information for predicting future transmission. Taken together, these quantitative findings formalize and support the asymmetry visible in the scatter plots. In other words, virulence has a detectable causal influence on subsequent transmission, while transmission provides only weak predictive information for future virulence. These inferences remain conditional on the quality and resolution of the observational data and are subject to potential biases from reporting errors, unobserved confounders and other sources of noise, which motivate follow up analyses with higher resolution co-variates and experimental validation.

Regional comparison of causal measures Applying LETR to the global SARS-CoV-2 time-series data revealed a particular set of relationships between virulence and transmission. But global pandemics are often defined by regional variation in their dynamics, which can be traced to any number of factors that differ from setting to setting. To assess whether the asymmetry observed in the global series is consistent across spatial (geographical) scales, we computed geometric information flows for three regional aggregates, and report the

summary measures in Table 4. Specifically, the causal influence of transmission on virulence is uniformly weak across all scales ($GeoC_{\beta \rightarrow \mu} = 0.0128$ globally and $0.0711 - 0.0919$ regionally), whereas the causal influence of virulence on transmission varies substantially, being comparatively strong at the global ($GeoC_{\mu \rightarrow \beta} = 0.2701$) and Asian (0.2460) scales but very weak in the USA (0.0246) and Europe (0.0420). The table indicates that virulence provides substantially more predictive information on future transmission at the global and Asian scales. The USA and Europe show comparatively smaller effects of virulence on transmission. In contrast, the causal influence of transmission on virulence remains weak across regions and is consistent with the global pattern. These regional differences may reflect variation in virus evolution, epidemic timing, behavior, socioeconomic status, reporting practices, or unobserved covariates [60, 61]. Detailed computational results for each region are reported in Section S1 of the Supplementary Information. Additional visualizations and supporting analyses are provided in the Supplementary Information.

Table 4. Summary of geometric information measures at regional and global scales. Values shown are $GeoC_{\beta \rightarrow \mu}$ (causal influence of transmission on virulence) and $GeoC_{\mu \rightarrow \beta}$ (causal influence of virulence on transmission). Lower values indicate weaker causal influence. Overall, the causal influence of transmission on virulence is markedly weaker. In the USA and Europe, virulence exerts only a very weak causal influence on transmission, whereas at the global and Asian scales virulence exerts a comparatively stronger influence. Full numerical results are provided in the Supplementary Information.

Region	$GeoC_{\beta \rightarrow \mu}$	$GeoC_{\mu \rightarrow \beta}$
Global	0.0128	0.2701
USA	0.0918	0.0246
Europe	0.0919	0.0420
Asia	0.0711	0.2460

3.2.2 Estimating invariant trait distributions for SARS-CoV-2 virulence and transmission

Generative maps for virulence and transmission may be inferred by regression. In this study, we fit one-step generative functions using the least absolute shrinkage and selection operator (LASSO) [62] and overlay the fitted maps on the data in Figures 4b and 4c. Because the chosen observables may not span the full causal state space, the fitted maps do not always capture all observed variability. Nonetheless, these maps are useful for short-term prediction and for formulating mechanistic hypotheses about trait updates. When the fitted map displays sensitive dependence on initial conditions, or when stochastic forcing is important, individual trajectories become unpredictable while the population-level distribution of trait values remains informative. In such cases, we estimate the transfer operator directly from data and derive long-term behavior from its invariant density. Practical, data-driven estimators include Ulam's method [63] and kernel-based estimators [64], which both approximate the Frobenius Perron operator and whose leading eigenvector yields the invariant density.

Estimated invariant densities computed by Ulam's method are shown in Figure 5b. The invariant density for virulence, plotted in Figure 5a, is bimodal with modes near $\mu \approx 0.0025$ and $\mu \approx 0.0175$. This pattern indicates that virulence values tend to concentrate at very low and slightly elevated levels in the long run. Possible explanations for this bimodality include the coexistence of distinct viral strains, heterogeneous vaccine coverage, or other ecological factors. The invariant density for transmission, shown in Figure 5b, is strongly concentrated near the lower end of the support and exhibits a rapidly decaying tail that resembles an exponential distribution for larger values. A weak secondary mode is apparent at the very low end of the transmission range. Taken together, the estimated densities suggest that, for the period and observables analyzed here, both virulence and transmission are more likely to occupy low values in the long term. A summary of the key insights from both the synthetic myxomatosis dataset and the SARS-CoV-2 case study, together with their broader implications for infectious disease research, is provided in Table 5.

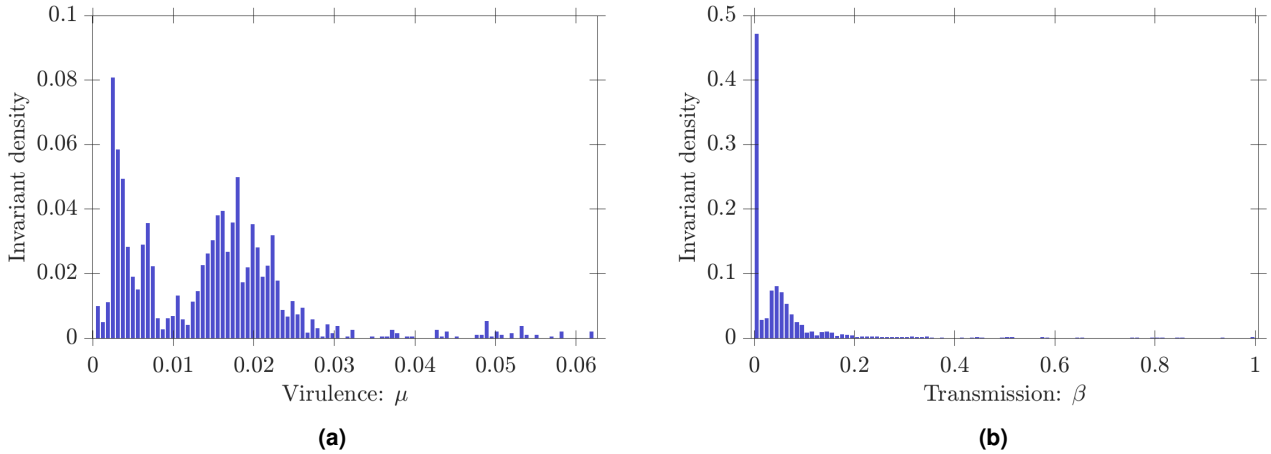


Fig. 5. Long-run trait distributions of SARS-CoV-2. Estimated invariant densities for SARS-CoV-2 virulence and transmission obtained by Ulam’s method. (a) The invariant density for virulence μ is bimodal with modes near $\mu \approx 0.0025$ and $\mu \approx 0.0175$. (b) The invariant density for transmission β , where β denotes the min-max scaled (see [65, 66]) daily new cases per million. The transmission density is strongly concentrated near the lower bound and displays a rapidly decaying tail that is approximately exponential, with a weak secondary mode at the very low end. Data are daily observations from Our World in Data [57, 58] covering the period from September 1st, 2020, to August 24, 2025. These estimates indicate a long-term tendency toward low virulence and low transmission. The observed bimodality in virulence may arise from variations in periods favorable to the pathogen, driven by host heterogeneities or environmental fluctuations.

4 Discussion

This study proposes *Granger-causality philosophy* as the basis of our proposed *learning evolutionary trait relationships* (LETR) framework. Contemporary causal inference is dominated by two complementary schools. One is the predictive, time-series oriented approach, originating from the Nobel Prize-winning work of Clive W.J. Granger [67], which tests whether past observations of one variable improve forecasts of another [19, 20]. The other is the interventionist or counterfactual approach epitomized by Pearl which formalizes causation in terms of hypothetical manipulations and do-calculus [15]. Bayesian network and causal graph methods have become increasingly popular across disciplines and have seen substantial uptake in biological applications [14, 68, 69, 70]. However, quantitative traits are naturally observed as time series and Granger style analysis aligns directly with forecasting goals and with the practical question of whether one trait improves the prediction of another [21, 22, 71].

LETR adopts the predictive information flow perspective. It also recognizes the continued value of interventionist and graphical approaches when experiments or explicit identification assumptions are available. In practice, we implement a geometric version of Granger style inference [43] because it provides a visual and quantitative complement to probabilistic measures such as transfer entropy [41]. Geometric diagnostics test whether the addition of a candidate predictor reduces the effective dimensionality of the one-step mapping, and thereby supplies information about the future of the focal variable. This approach avoids some technical limitations of entropy-based estimators and is particularly useful when interactions are strongly nonlinear or when low-dimensional structure is present in the data. Geometric methods also facilitate intuitive exploratory analysis and hypothesis generation for downstream, more assumption-heavy Granger causality tests.

We apply this to a long-standing pillar of disease evolution and ecology: the relationship between virulence and transmission in pathogen-host interactions. Our findings demonstrate that causal structure among pathogen traits is dynamically asymmetric and scale-dependent, generating stable evolutionary attractors that cannot be captured by tradeoff theory or correlational analyses alone.

Case study I: Myxomatosis outbreak-inspired synthetic data In the myxomatosis-inspired system, case mortality modifies within-host titers, which determine the time course of infectiousness, and the probability of infection from disease vectors (hematophagous insects). This mechanistic chain informed our synthetic design

Table 5. Comparison of key elements of LETR across the synthetic benchmark (myxomatosis-motivated) and SARS-CoV-2 applications, highlighting shared and distinct causal patterns in virulence–transmission dynamics.

Element	Case study I: Synthetic benchmark (myxomatosis-motivated)	Case study II: pandemic application	Implications for disease evolution and ecology
Predictive relationship	LETR recovers the imposed directional influence and demonstrates that virulence drives transmission.	In SARS-CoV-2 data, the inferred direction varies by scale and setting. In some aggregates virulence precedes transmission, while elsewhere the effect is very weak or absent. This pattern likely reflects biological mechanisms and setting specific factors such as epidemic phase, behavior, testing and reporting. Causal claims therefore require local diagnostics.	Virulence → transmission is dynamically asymmetric and scale-dependent. Monitoring virulence can improve short term forecasts in some settings but inference requires corroboration with local data on behavior, testing and reporting.
Trait interdependence	Geometric diagnostics capture how traits co-vary in synthetic systems.	In this regime, transmission and virulence alone do not fully explain the behavior of epidemics.	Indicates that complex trait coupling demands multi-trait models.
Long-term distributions	Simulations produce chaotic attractors for virulence and transmission consistent with benchmark design.	Virulence shows a bimodal distribution (modes near 0.0025 and 0.0175); transmission is low with an exponential-like tail.	Reveals distinct evolutionary or ecological regimes influencing virulence outcomes.
Possible mechanisms	Framework recovers known mechanistic directionality from imposed system.	Peaks in virulence may reflect different viral strains or host-specific responses.	Highlights capacity to identify mechanistic heterogeneity from observational data.
Analytical contribution	LETR pipeline demonstrates causal discovery using geometric diagnostics.	“Invariant-density” estimates provide compact summaries of long-term behavior.	Integrates causal inference with dynamical-systems diagnostics for predictive epidemiology.

and provided a clear ground truth for testing LETR. Applying LETR to the synthetic data, we identified Granger style predictors with geometric diagnostics and correlation dimension estimates. Geometric causal measures recovered the imposed directional influence from virulence to transmission and confirmed that transmission does not causally drive virulence. The synthetic validation demonstrates two concrete uses of LETR for the empirical myxomatosis problem. Firstly, LETR tests whether observed trait time series are consistent with virulence acting upstream of transmission by asking whether inclusion of virulence substantially reduces the dimension of the predictive manifold and improves one-step forecasts. Second, LETR provides quantitative evidence for directional influence that can be aligned with mechanistic intuition from within host to population level dynamics. Extensions that detect indirect pathways such as causation entropy can be layered into LETR to explicitly test whether within host titer mediates the effect of virulence on transmission [42]. Together these steps show how the mechanistic intuition from myxomatosis can be translated into concrete, data driven tests that yield testable epidemiological patterns and insights. The implications of these patterns for disease evolution and ecology are summarized in Table 5.

Case study II: Modern pandemic using SARS-CoV-2 epidemiological data Applying LETR to the global SARS-CoV-2 series, we find that changes in virulence μ generally provide more predictive information for subsequent transmission β than the reverse. This asymmetry is strongest at the global scale and in Asia and weaker in the USA and Europe. The information flow from transmission to virulence remains weak across regions. The

patterns and their implications for disease evolution and ecology are summarized in Table 5. Further methodological details and per-region supporting analyses are provided in Section 3.2.1 and Supplementary Information Section S1.

Estimated invariant densities indicate long-term tendencies toward low virulence and low transmission. Specifically, virulence is bimodal with modes near $\mu \approx 0.0025$ and $\mu \approx 0.0175$, while transmission β is strongly concentrated below 0.2 with an approximately exponential tail Figure 5. The bimodality in virulence may reflect the coexistence of distinct viral lineages, or it may arise from host-level heterogeneity, including behavioral, social, and ecological factors that shape exposure and outcomes [22, 69]. High virulence episodes can also lead to increased public awareness, vaccination, and other interventions that suppress both severity and transmission which aligns with the asymmetric causal pattern we observe [5, 72, 73]. Social inequalities and spatial clustering of vulnerable individuals can sustain systematic differences in severity across subpopulations [74, 75, 76, 77]. Finally, environmental variation that alters the duration of periods favorable to the pathogen can produce a mix of rare severe outbreaks and frequent mild outbreaks, generating a bimodal long-term distribution [78].

Implications for the ecology and evolution of infectious disease Through simulated and real-world pandemic examples, we observe the peculiar nature of the relationship between virulence and transmission. Far from being a theoretical exercise, the findings offer a careful means of advancing a subversive idea: traits assumed to be the product of evolutionary forces can also be driven by ecological or behavioral factors. This underscores the need to consider the statistical concept of model identifiability—where differing model structures can fit a given epidemiological time-series curve [79, 80]—when inferring the forces driving virulence, transmission, and the shape of epidemics. That is, one can mistakenly interpret changes in virulence and/or transmission as the result of molecular evolution when those changes very well could have arisen from non-genetic (e.g., ecological) forces. These findings implore us to think carefully about the relationship between virulence and transmission, and reconcile the evolutionary and ecological forces as fundamental (often co-occurring) shapers of disease dynamics. Relatedly, our results highlight the need for fine-grained genetic, clinical, and field data to resolve patterns such as the dual virulence peaks observed for SARS-CoV-2. They also motivate integrating modeling and empirical surveillance with ecological and mechanistic studies to strengthen causal inference between traits of interest.

Conclusions As a general-purpose, data-driven framework, LETR opens new avenues for mechanistic understanding and predictive modeling in the era of large data sets. This allows researchers not only to ask “which traits drive others,” but also to answer “what trait diversity will emerge over time” (as characterized by the invariant density derived from transfer operators). This unified approach connects mechanistic causality with population-level patterns, bridging the gap between individual-level trait dynamics and macro-scale outcomes.

Although our study focused on the relationship between virulence and transmission, the LETR framework can be extended to other trait pairings. For instance, LETR can be used to identify causal relationships between traits and to quantify how covariates such as ecological context, host demography, and treatment regimes influence these relationships. Potential applications include: antibiotic resistance versus growth rate [81]; host resistance versus tolerance [82]; life-history tradeoffs between growth and reproduction [55]; and phenotypic plasticity versus canalization [83]. Consequently, the same underlying trait pairing can manifest differently under specific conditions [11].

Acknowledgments

The authors would like to thank the 2024 and 2025 meetings of the Society for Modeling and Theory in Population Biology, where ideas germane to this article were discussed and developed. The authors thank members of the OGplexus for helpful feedback on various aspects of the project.

Funding

This work was supported by the Santa Fe Institute and the Mynoon and Stephen Doro MD, PhD Family Private Foundation Fund.

Data availability

Data and code are available on Git: <https://github.com/OgPlexus/learningvirulence>

Author Contributions

SS and CBO conceived the study, developed the models, interpreted the results, and wrote the original and revised versions of the manuscript.

References

- [1] Ben Longdon, Jarrod D Hadfield, Jonathan P Day, Sophia CL Smith, John E McGonigle, Rodrigo Cogni, Chuan Cao, and Francis M Jiggins. “The causes and consequences of changes in virulence following pathogen host shifts”. In: *PLoS pathogens* 11.3 (2015), e1004728.
- [2] Roy M Anderson and Robert M May. “Coevolution of hosts and parasites”. In: *Parasitology* 85.2 (1982), pp. 411–426.
- [3] Paul W Ewald. “Host-parasite relations, vectors, and the evolution of disease severity”. In: *Annual Review of Ecology and Systematics* 14 (1983), pp. 465–485.
- [4] Richard E Lenski. “Evolution of plague virulence”. In: *Nature* 334.6182 (1988), pp. 473–474.
- [5] James J Bull. “Virulence”. In: *Evolution* 48.5 (1994), pp. 1423–1437.
- [6] Andrew F Read. “The evolution of virulence”. In: *Trends in microbiology* 2.3 (1994), pp. 73–76.
- [7] Samuel Alizon, Amy Hurford, Nicole Mideo, and Minus Van Baalen. “Virulence evolution and the trade-off hypothesis: history, current state of affairs and the future”. In: *Journal of evolutionary biology* 22.2 (2009), pp. 245–259.
- [8] Ketty Kabengele, Wendy C Turner, Paul E Turner, and C Brandon Ogbunugafor. “A meta-analysis highlights the idiosyncratic nature of tradeoffs in laboratory models of virus evolution”. In: *Virus Evolution* 10.1 (2024), veae105.
- [9] Charlotte Rafaluk-Mohr. “The relationship between parasite virulence and environmental persistence: a meta-analysis”. en. In: *Parasitology* 146.07 (June 2019), pp. 897–902. issn: 0031-1820, 1469-8161. url: https://www.cambridge.org/core/product/identifier/S0031182019000015/type/journal_article (visited on 10/06/2021).
- [10] Miguel A Acevedo, Forrest P Dillemuth, Andrew J Flick, Matthew J Faldyn, and Bret D Elderd. “Virulence-driven trade-offs in disease transmission: A meta-analysis”. In: *Evolution* 73.4 (2019), pp. 636–647.
- [11] Gregor F Fussmann, Michel Loreau, and Peter A Abrams. “Eco-evolutionary dynamics of communities and ecosystems”. In: *Functional ecology* (2007), pp. 465–477.
- [12] Nita Bharti. “Linking human behaviors and infectious diseases”. In: *Proceedings of the National Academy of Sciences* 118.11 (2021), e2101345118.
- [13] Grier P Page, Varghese George, Rodney C Go, Patricia Z Page, and David B Allison. ““Are we there yet?”: Deciding when one has demonstrated specific genetic causation in complex diseases and quantitative traits”. In: *The American Journal of Human Genetics* 73.4 (2003), pp. 711–719.
- [14] Tobias Kurth. *Continuing to advance epidemiology*. 2021.
- [15] Judea Pearl. “Causal inference”. In: *Causality: objectives and assessment* (2010), pp. 39–58.
- [16] Trudy FC Mackay, Eric A Stone, and Julien F Ayroles. “The genetics of quantitative traits: challenges and prospects”. In: *Nature Reviews Genetics* 10.8 (2009), pp. 565–577.
- [17] A Battle and SB Montgomery. “Determining causality and consequence of expression quantitative trait loci”. In: *Human genetics* 133.6 (2014), pp. 727–735.
- [18] Trond Reitan. “Layeranalyzer: inferring correlative and causal connections from time series data in R”. In: *Methods in Ecology and Evolution* (2019).
- [19] Clive WJ Granger. “Investigating causal relations by econometric models and cross-spectral methods”. In: *Econometrica: journal of the Econometric Society* (1969), pp. 424–438.
- [20] Norbert Wiener. “The theory of prediction”. In: *Mathematics for the Engineer* (1956).
- [21] Shuixia Guo, Christophe Ladroue, and Jianfeng Feng. “Granger causality: theory and applications”. In: *Frontiers in computational and systems biology*. Springer, 2010, pp. 83–111.

[22] Ethan R Deyle, M Cyrus Maher, Ryan D Hernandez, Sanjay Basu, and George Sugihara. "Global environmental drivers of influenza". In: *Proceedings of the National Academy of Sciences* 113.46 (2016), pp. 13081–13086.

[23] Joseph NS Eisenberg, Manish A Desai, Karen Levy, Sarah J Bates, Song Liang, Kyra Naumoff, and James C Scott. "Environmental determinants of infectious disease: a framework for tracking causal links and guiding public health research". In: *Environmental health perspectives* 115.8 (2007), pp. 1216–1223.

[24] Mervyn Susser and Ezra Susser. "Choosing a future for epidemiology: II. From black box to Chinese boxes and eco-epidemiology." In: *American journal of public health* 86.5 (1996), pp. 674–677.

[25] James S Koopman and John W Lynch. "Individual causal models and population system models in epidemiology." In: *American journal of public health* 89.8 (1999), pp. 1170–1174.

[26] Brian C. Saul. "Causal Inference in the Study of Infectious Disease". In: *Oxford Research Encyclopedia of Global Public Health*. Oxford University Press, 2017.

[27] Nancy Krieger. "Theories for social epidemiology in the 21st century: an ecosocial perspective". In: *International journal of epidemiology* 30.4 (2001), pp. 668–677.

[28] Donald Rubin. "Estimating causal effects of treatments in experimental and observational studies". In: *Ets research bulletin series* 1972.2 (1972), pp. i–31.

[29] M. Elizabeth Halloran and Michael G. Hudgens. "Causal Inference for Vaccine Effects on Infectiousness". In: *International Journal of Biostatistics* 8.2 (2012), p. 1354. doi: [10.2202/1557-4679.1354](https://doi.org/10.2202/1557-4679.1354).

[30] Tyler J. VanderWeele and Eric J. Tchetgen Tchetgen. "Components of the indirect effect in vaccine trials". In: *Epidemiology* 23.4 (2012), pp. 640–647.

[31] Joseph NS Eisenberg, Bryan L Lewis, Travis C Porco, Alan H Hubbard, and John M Colford Jr. "Bias due to secondary transmission in estimation of attributable risk from intervention trials". In: *Epidemiology* 14.4 (2003), pp. 442–450.

[32] James M Robins, Miguel Angel Hernan, and Babette Brumback. *Marginal structural models and causal inference in epidemiology*. 2000.

[33] M Elizabeth Halloran and Claudio J Struchiner. "Causal inference in infectious diseases". In: *Epidemiology* (1995), pp. 142–151.

[34] George Sugihara, Robert May, Hao Ye, Chih-hao Hsieh, Ethan Deyle, Michael Fogarty, and Stephan Munch. "Detecting causality in complex ecosystems". In: *science* 338.6106 (2012), pp. 496–500.

[35] Owen R Liu and Steven D Gaines. "Environmental context dependency in species interactions". In: *Proceedings of the National Academy of Sciences* 119.36 (2022), e2118539119.

[36] RA Ranga Prabodanvie, Sergei Schreider, Bernard Cazelles, and Lewi Stone. "Coherence of dengue incidence and climate in the wet and dry zones of Sri Lanka". In: *Science of the Total Environment* 724 (2020), p. 138269.

[37] Md Jamal Hossain, Nazia Sultana, Anwesha Das, Fariea Nazim Jui, Md Kamrul Islam, Md Mijanoor Rahman, and Mohammad Mafizur Rahman. "Analysis of effects of meteorological variables on dengue incidence in Bangladesh using VAR and Granger causality approach". In: *Frontiers in Public Health* 12 (2024), p. 1488742.

[38] Aline Foerster Grande, Guilherme Pumi, and Gabriela Bettella Cybis. "Granger causality and time series regression for modelling the migratory dynamics of influenza into Brazil". In: *SORT (Statistics and Operations Research Transactions). spain, Barcelona Institut d'Estadística de Catalunya*. Vol. 46 (2022), p. 161-188 (2023).

[39] Afrina Andriani Sebayang, Muhammad Fakhruddin, Mia Siti Khumaero, Hilda Fahlena, Chai Jian Tay, Su Yean Teh, Ardhasena Sopaheluwakan, Nuning Nuraini, and Edy Soewono. "Unraveling the impact of human mobility on dengue outbreaks in Peninsular Malaysia: a Granger causality approach". In: *International Journal of Environmental Health Research* (2025), pp. 1–16.

[40] Carolina Romero García, Álvaro Briz-Redón, Adina Iftimi, Manuel Lozano, José De Andrés, Giovanni Landoni, and Massimiliano Zanin. "Understanding small-scale COVID-19 transmission dynamics with the Granger causality test". In: *Archives of Environmental & Occupational Health* 78.5 (2023), pp. 273–281.

[41] Thomas Schreiber. "Measuring information transfer". In: *Physical review letters* 85.2 (2000), p. 461.

[42] Jie Sun and Erik M Bollt. "Causation entropy identifies indirect influences, dominance of neighbors and anticipatory couplings". In: *Physica D: Nonlinear Phenomena* 267 (2014), pp. 49–57.

[43] Sudam Surasinghe and Erik M Bollt. "On geometry of information flow for causal inference". In: *Entropy* 22.4 (2020), p. 396.

[44] Robert M May. "Simple mathematical models with very complicated dynamics". In: *Nature* 261.5560 (1976), pp. 459–467.

[45] Jacob C Koella and Michael Doebeli. "Population dynamics and the evolution of virulence in epidemiological models with discrete host generations". In: *Journal of Theoretical Biology* 198.3 (1999), pp. 461–475.

[46] Greg Dwyer, Simon A Levin, and Linda Buttell. "A simulation model of the population dynamics and evolution of myxomatosis". In: *Ecological monographs* 60.4 (1990), pp. 423–447.

[47] Andrzej Lasota and Michael C Mackey. *Chaos, Fractals, and Noise: Stochastic Aspects of Dynamics*. Vol. 97. Springer Science & Business Media, 1998.

[48] Erik M Bollt. "Controlling chaos and the inverse Frobenius–Perron problem: global stabilization of arbitrary invariant measures". In: *International Journal of Bifurcation and Chaos* 10.05 (2000), pp. 1033–1050.

[49] Frank Fenner and F. N. Ratcliffe. *Myxomatosis*. Cambridge: Cambridge University Press, 1965.

[50] Peter J. Kerr. "Myxomatosis in Australia and Europe: A model for emerging infectious diseases". In: *Antiviral Research* 93.3 (2012), pp. 387–415. doi: [10.1016/j.antiviral.2012.01.009](https://doi.org/10.1016/j.antiviral.2012.01.009).

[51] Frank Fenner. "Changes in the mortality-rate due to myxomatosis in the Australian wild rabbit". In: *Nature* 172 (1953), pp. 228–230. doi: [10.1038/172228a0](https://doi.org/10.1038/172228a0).

[52] I. D. Marshall and Frank Fenner. "Studies in the epidemiology of infectious myxomatosis of rabbits: V. Changes in the innate resistance of Australian wild rabbits exposed to myxomatosis". In: *Journal of Hygiene* 56.2 (1958), pp. 288–302. doi: [10.1017/s0022172400037773](https://doi.org/10.1017/s0022172400037773).

[53] Peter J. Kerr, Elodie Ghedin, Jay V. DePasse, Alex Fitch, Isabella M. Cattadori, Peter J. Hudson, David C. Tscharke, Andrew F. Read, and Edward C. Holmes. "Evolutionary History and Attenuation of Myxoma Virus on Two Continents". In: *PLOS Pathogens* 8.10 (2012), e1002950. doi: [10.1371/journal.ppat.1002950](https://doi.org/10.1371/journal.ppat.1002950).

[54] Frank Fenner, M. F. Day, and Gwendolyn M. Woodrooffe. "Epidemiological consequences of the mechanical transmission of myxomatosis by mosquitoes". In: *Journal of Hygiene* 54.2 (1956), pp. 284–303. doi: [10.1017/s0022172400044351](https://doi.org/10.1017/s0022172400044351).

[55] Stephen C Stearns. *The evolution of life histories*. Oxford university press, 1998.

[56] The MathWorks, Inc. *correlationDimension: Measure of chaotic signal complexity*. <https://www.mathworks.com/help/predmait/ref/correlationdimension.html>. 2025.

[57] Edouard Mathieu, Hannah Ritchie, Lucas Rodés-Guirao, Cameron Appel, Daniel Gavrilov, Charlie Giattino, Joe Hasell, Bobbie Macdonald, Saloni Dattani, Diana Beltekian, Esteban Ortiz-Ospina, and Max Roser. *Mortality Risk of COVID-19*. Our World in Data. Online: <https://ourworldindata.org/mortality-risk-covid>. 2020.

[58] Edouard Mathieu, Hannah Ritchie, Lucas Rodés-Guirao, Cameron Appel, Daniel Gavrilov, Charlie Giattino, Joe Hasell, Bobbie Macdonald, Saloni Dattani, Diana Beltekian, Esteban Ortiz-Ospina, and Max Roser. *COVID-19 Cases*. Our World in Data. Online: <https://ourworldindata.org/covid-cases>. 2020.

[59] Dilber Uzun Ozsahin, Mubarak Taiwo Mustapha, Auwalu Saleh Mubarak, Zubaida Said Ameen, and Berna Uzun. "Impact of feature scaling on machine learning models for the diagnosis of diabetes". In: *2022 International Conference on Artificial Intelligence in Everything (AIE)*. IEEE. 2022, pp. 87–94.

[60] Jing Pan, Arivizhivendhan Kannan Villalan, Guanying Ni, Renna Wu, ShiFeng Sui, Xiaodong Wu, and XiaoLong Wang. "Assessing eco-geographic influences on COVID-19 transmission: a global analysis". In: *Scientific Reports* 14.1 (2024), p. 11728.

[61] Sebastien Bourdin and Nadine Levratto. "Regional implications of COVID-19". In: *International Regional Science Review* 46.5-6 (2023), pp. 515–522.

[62] Robert Tibshirani. "Regression shrinkage and selection via the lasso". In: *Journal of the Royal Statistical Society Series B: Statistical Methodology* 58.1 (1996), pp. 267–288.

[63] Stanislaw M. Ulam. *A Collection of Mathematical Problems*. Interscience Publishers, 1960, p. 150.

[64] Sudam Surasinghe, Jeremie Fish, and Erik M Boltt. "Learning transfer operators by kernel density estimation". In: *Chaos: An Interdisciplinary Journal of Nonlinear Science* 34.2 (2024).

[65] Y Kumar Jain and Santosh Kumar Bhandare. "Min max normalization based data perturbation method for privacy protection". In: *International Journal of Computer & Communication Technology* 2.8 (2011), pp. 45–50.

[66] Peshawa J Muhammad Ali. "Investigating the Impact of min-max data normalization on the regression performance of K-nearest neighbor with different similarity measurements". In: *ARO-The Scientific Journal of Koya University* 10.1 (2022), pp. 85–91.

[67] David F. Hendry. "The Nobel Memorial Prize for Clive W. J. Granger". In: *Scand. J. Econ* 106.2 (2004), pp. 187–213.

[68] Zachary M Laubach, Eleanor J Murray, Kim L Hoke, Rebecca J Safran, and Wei Perng. "A biologist's guide to model selection and causal inference". In: *Proceedings of the Royal Society B* 288.1943 (2021), p. 20202815.

[69] Laura Andrea Barrero Guevara, Sarah C Kramer, Tobias Kurth, and Matthieu Domenech de Cellès. "Causal inference concepts can guide research into the effects of climate on infectious diseases". In: *Nature Ecology & Evolution* 9.2 (2025), pp. 349–363.

[70] Bill Shipley. "Testing causal explanations in organismal biology: causation, correlation and structural equation modelling". In: *Oikos* (1999), pp. 374–382.

[71] Jakob Runge, Sebastian Bathiany, Erik Boltt, Gustau Camps-Valls, Dim Coumou, Ethan Deyle, Clark Glymour, Marlene Kretschmer, Miguel D Mahecha, Jordi Muñoz-Marí, et al. "Inferring causation from time series in Earth system sciences". In: *Nature communications* 10.1 (2019), p. 2553.

[72] Laura Fierce, Alison J Robey, and Cathrine Hamilton. "High efficacy of layered controls for reducing exposure to airborne pathogens". In: *Indoor air* 32.2 (2022), e12989.

[73] Jacobus C De Roode, Andrew J Yates, and Sonia Altizer. "Virulence-transmission trade-offs and population divergence in virulence in a naturally occurring butterfly parasite". In: *Proceedings of the national academy of sciences* 105.21 (2008), pp. 7489–7494.

[74] Paul Farmer. "Social inequalities and emerging infectious diseases". In: *Understanding and applying medical anthropology* (2016), pp. 118–126.

[75] Sanne Muurling, Tim Riswick, and Katalin Buzasi. "The last nationwide smallpox epidemic in the Netherlands: Infectious disease and social inequalities in Amsterdam, 1870–1872". In: *Social Science History* 47.2 (2023), pp. 189–216.

[76] Sudam Surasinghe, Swathi Nachiar Manivannan, Samuel V Scarpino, Lorin Crawford, and C Brandon Ogbunugafor. "Structural causal influence (sci) captures the forces of social inequality in models of disease dynamics". In: *arXiv preprint arXiv:2409.09096* (2024).

- [77] Neil W Blackstone, Sarah R Blackstone, and Anne T Berg. “Variation and multilevel selection of SARS-CoV-2”. In: *Evolution* 74.10 (2020), pp. 2429–2434.
- [78] Jani Anttila, Veijo Kaitala, Jouni Laakso, and Lasse Ruokolainen. “Environmental variation generates environmental opportunist pathogen outbreaks”. In: *PLoS One* 10.12 (2015), e0145511.
- [79] Michael H Cortez and Joshua S Weitz. “Distinguishing between indirect and direct modes of transmission using epidemiological time series”. In: *The American Naturalist* 181.2 (2013), E43–E52.
- [80] S. Vajda and H. Rabitz. “Identifiability and distinguishability of first-order reaction systems”. In: *The Journal of Physical Chemistry* 92.3 (Feb. 1988), pp. 701–707. issn: 1541-5740. doi: [10.1021/j100314a024](https://doi.org/10.1021/j100314a024). URL: <http://dx.doi.org/10.1021/j100314a024>.
- [81] Mehrose Ahmad, Sai Varun Aduru, Robert P Smith, Zirui Zhao, and Allison J Lopatkin. “The role of bacterial metabolism in antimicrobial resistance”. In: *Nature Reviews Microbiology* (2025), pp. 1–16.
- [82] Lars Råberg, Derek Sim, and Andrew F Read. “Disentangling genetic variation for resistance and tolerance to infectious diseases in animals”. In: *Science* 318.5851 (2007), pp. 812–814.
- [83] Giuseppe Fusco and Alessandro Minelli. *Phenotypic plasticity in development and evolution: facts and concepts*. 2010.

Supporting Information for

Learning virulence-transmission relationships using causal inference

Sudam Surasinghe^{1,2}✉ and C. Brandon Ogbunugafor^{1,2,3}✉

¹Department of Ecology & Evolutionary Biology, Yale University, New Haven, CT 06520, USA

²Public Health Modeling Unit, Yale School of Public Health, New Haven, CT 06510, USA

³Santa Fe Institute, Santa Fe, NM 87501, USA

✉S.S.: sudam.surasinghe@yale.edu; C.B.O: brandon.ogbunu@yale.edu

This PDF file includes:

1	Introduction	1
2	Methods	2
2.1	Identify Granger causal variables	4
2.2	Learning virulence using discrete maps and transfer operators	5
3	Results	6
3.1	Case study I: Causal model for virulence and transmission in a synthetic dataset of myxomatosis	7
3.1.1	Simulated virulence and transmission dynamics	7
3.1.2	Visualizing simulated data to identify Granger causal relationships	8
3.1.3	Testing causal variables for virulence in synthetic data	9
3.1.4	Testing causal variables for transmission in synthetic data	10
3.2	Case study II: LETR analysis of causality and invariant distributions in a modern pandemic dataset	11
3.2.1	Causal discovery of virulence–transmission dynamics in SARS-CoV-2	11
3.2.2	Estimating invariant trait distributions for SARS-CoV-2 virulence and transmission	14
4	Discussion	15
S5	Results for SARS-CoV-2	25
S5.1	Region-specific causal analyses	26
S5.1.1	Results of regional causal analysis	26
S6	Supplementary notes and figures on the LETR study	31
S6.1	Study limitations	31
S6.2	Supplementary Figures	31
S6.2.1	Causal model for Granger style predictor testing	31
S6.2.2	Pathogen passage schematics and ensemble distributions	31
S6.2.3	Simulated time series data synthetic example and causal model	32
S7	Dynamics of virulence as a logistic map	34
S7.1	Chaos in the logistic map and long-term trait distributions	34

S5 Results for SARS-CoV-2

In the main text, we analyze SARS-CoV-2 at the global level. As noted there, the results may be affected by numerous co-variates, which makes the causal relationship between virulence and transmission appear weak in an aggregated setting. This highlights the extent to which these relationships are context-dependent. Many of these co-variates, including environmental conditions, behavioral patterns, public health policies, and socio-cultural factors, can be mitigated when the analysis is conducted at the country or regional level. To illustrate this, the present supporting materials provide parallel analyses for the United States, Europe, and Asia.

Time series of SARS-CoV-2 virulence and transmission

For completeness, we present the raw time series used in the analysis for both global and selected regional aggregates. The daily case fatality rate (CFR) is used as a proxy for virulence, and transmission is measured by daily new cases per million people rescaled to the unit interval using min–max normalization. The figure displays a global (top) and three compact regional panels (bottom) showing the USA, Europe, and Asia. In the plots, CFR is shown in black and transmission in blue. The series follows the available data range [1, 2], and provide empirical input for the subsequent LETR analysis.

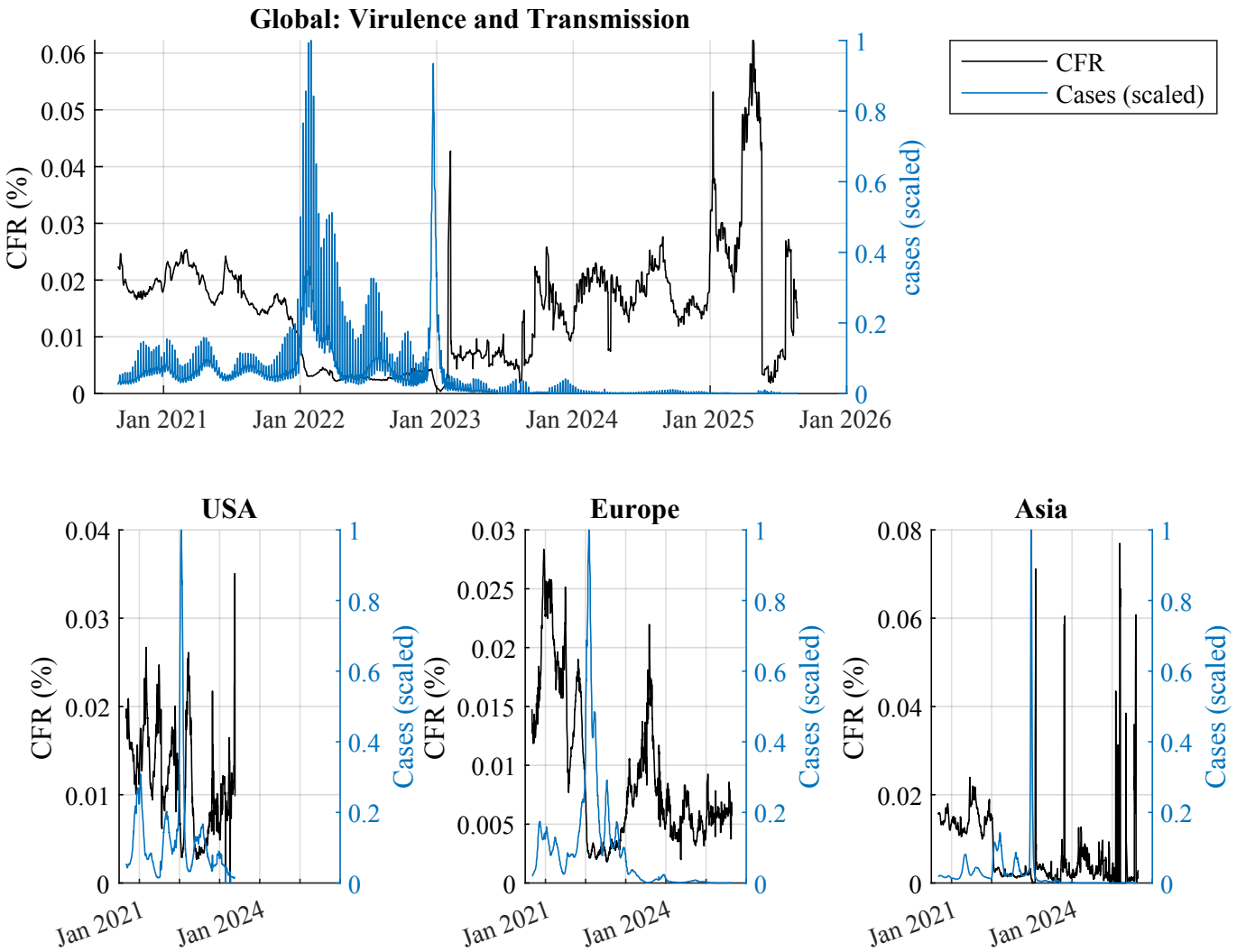


Fig. S1. Time series of SARS-CoV-2 virulence and transmission. The top panel shows global CFR (left axis, black) and transmission (right axis, daily new cases per million, min–max scaled to [0, 1], blue). The three lower panels present the corresponding regional series for the USA, Europe, and Asia, plotted using the same color convention. Each regional panel uses its own available date range following the data in [1, 2].

S5.1 Region-specific causal analyses

The following sections present the region-by-region analyses that parallel the global workflow described in the main text. Each regional subsection reproduces the same diagnostic pipeline used for the global data and provides scatterplots, low-dimensional geometry diagnostics, and conditional geometric information flow measures. The objective is to assess whether the asymmetry between virulence and transmission documented at the global level persists at regional scales and to identify region-specific features that may inform mechanistic hypotheses.

Data and proxies For each region, we analyze two primary series. Virulence is measured by the daily case fatality rate (CFR), computed as the number of confirmed deaths divided by the number of confirmed cases on the same reporting date unless otherwise stated. Transmission is measured by the daily new confirmed cases per million people. Transmission series are min–max scaled to the unit interval $[0, 1]$. Where relevant, each regional panel uses the local date vector for that region [1, 2].

Analytical methods The results reported here are obtained by applying the same analytical pipeline described in the main text. In brief:

- Pairwise scatterplots of μ_n vs μ_{n+1} and β_n vs β_{n+1} are used to visually inspect low-dimensional structure and predictive geometry.
- Correlation dimension $D_2(\cdot)$ estimates are computed with MATLAB's `correlationDimension` routine [3].
- Geometric information flow measures are computed following the procedure described in the Methods. We report both conditional geometric information measures and derived directional geometric information flow quantities. For example, we evaluate $\text{GeoC}(\mu_{n+1} | \mu_n)$ and $\text{GeoC}(\mu_{n+1} | \mu_n, \beta_n)$, and we compute directional flow measures such as $\text{GeoC}_{\beta \rightarrow \mu} = \text{GeoC}(\mu_{n+1} | \mu_n) - \text{GeoC}(\mu_{n+1} | \mu_n, \beta_n)$.

S5.1.1 Results of regional causal analysis

Here, we summarize the regional estimates of correlation dimension and geometric information flow in Table S1, with corresponding phase space and one-step scatterplots shown in Figures S2 to S4. These results allow a direct comparison with the global analysis reported in the main text.

Table S1. Selected geometric information measures by region. Values correspond to correlation dimension D_2 and conditional geometric information $GeoC$. Here, $GeoC_{x \rightarrow y}$ denotes the geometric information flow measure used to assess causal influence from x to y as described in Methods section 2.1 of the main text. The D_2 estimates were computed with MATLAB's `correlationDimension` function and parameters were selected by visual inspection of the function's interactive log–log plot of the correlation sum against neighbourhood radius. Reported values are rounded to six decimal places. Overall, the measures indicate that transmission exerts a weak causal influence on virulence at both global and regional scales. For the USA and Europe, virulence also shows a weak causal influence on transmission. By contrast, at the global and Asia scales, virulence exerts a relatively stronger causal influence on transmission.

Term	Global	USA	Europe	Asia
$D_2(\mu_n)$	0.960042	0.950158	0.927558	0.899594
$D_2([\mu_n, \mu_{n+1}])$	1.072071	1.095456	1.215081	1.153344
$D_2([\mu_n, \beta_n, \mu_{n+1}])$	1.371026	1.533408	1.537789	1.337165
$D_2([\mu_n, \beta_n])$	1.271778	1.479956	1.342144	1.154491
$D_2(\beta_n)$	0.693734	0.892532	0.795365	0.737713
$D_2([\beta_n, \beta_{n+1}])$	1.001665	1.074973	0.854573	1.004846
$D_2([\mu_n, \beta_n, \beta_{n+1}])$	1.309606	1.637780	1.359345	1.188627
$GeoC(\mu_{n+1} \mid \mu_n)$	0.112029	0.145298	0.287523	0.25375
$GeoC(\mu_{n+1} \mid \mu_n, \beta_n)$	0.099248	0.053452	0.195645	0.182674
$GeoC_{\beta \rightarrow \mu}$	0.012781	0.091846	0.091878	0.071076
$GeoC(\beta_{n+1} \mid \beta_n)$	0.307931	0.182441	0.059208	0.267133
$GeoC(\beta_{n+1} \mid \beta_n, \mu_n)$	0.037828	0.157824	0.017201	0.021098
$GeoC_{\mu \rightarrow \beta}$	0.270103	0.024617	0.042007	0.246035

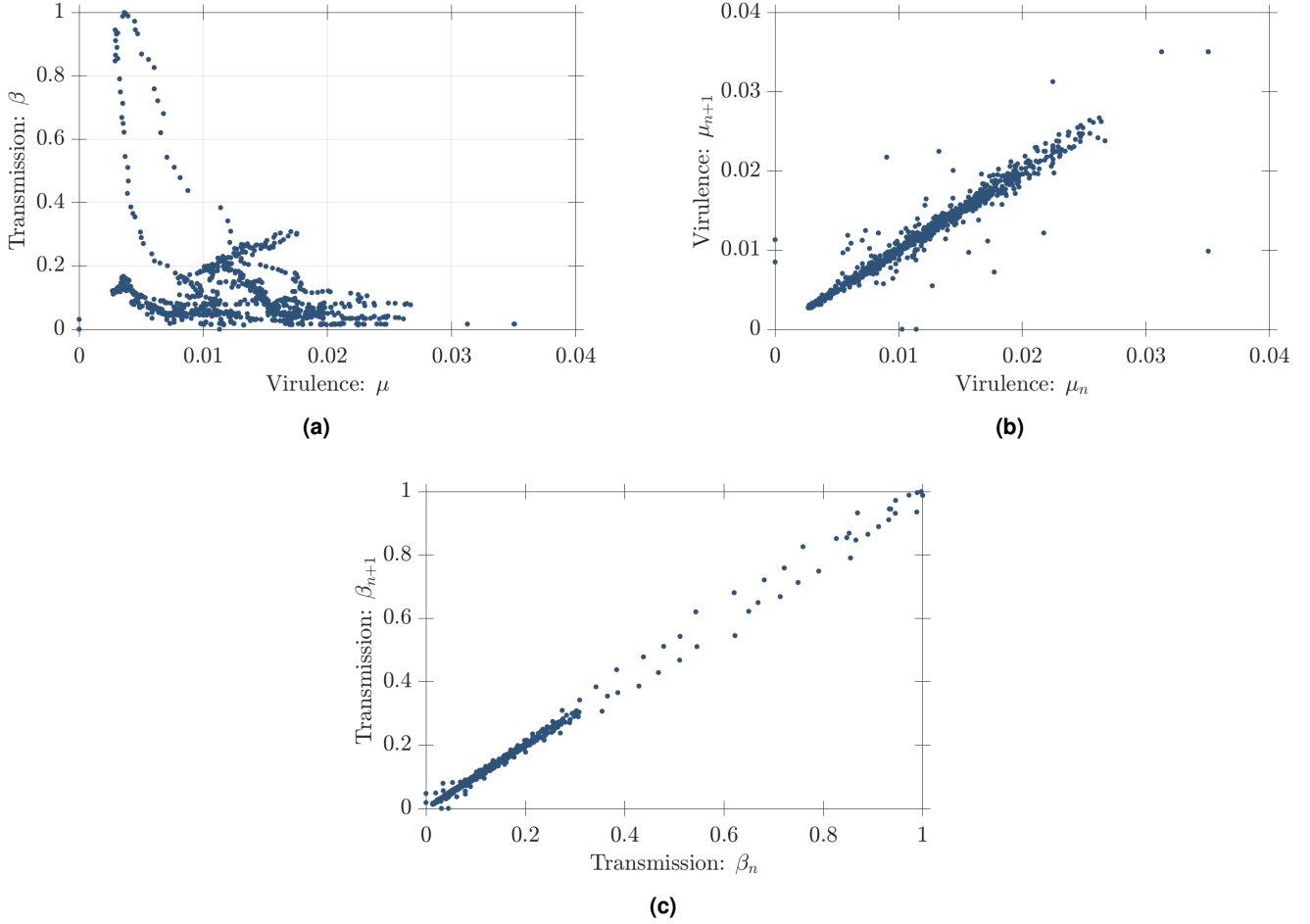


Fig. S2. Geometric investigation of SARS-CoV-2 trait dynamics for the United States. One-step relationships show that both virulence and transmission are largely self-predictive. The USA data are daily observations from Our World in Data [1, 2] covering the period from September 1st, 2020, to May 22nd, 2023. (a) shows the joint phase space of virulence μ and transmission β . (b) shows μ_{n+1} plotted against μ_n . The horizontal axis shows μ_n and the vertical axis shows μ_{n+1} , which emphasizes short-term predictability of virulence. (c) shows β_{n+1} plotted against β_n . In contrast to the global transmission data (see main text section 3.2.1, Figure 4c), where higher transmission values separate into three apparent branches, the USA transmission series lacks that branching. This observation suggests a reduced role for additional causal drivers of transmission at the national level.

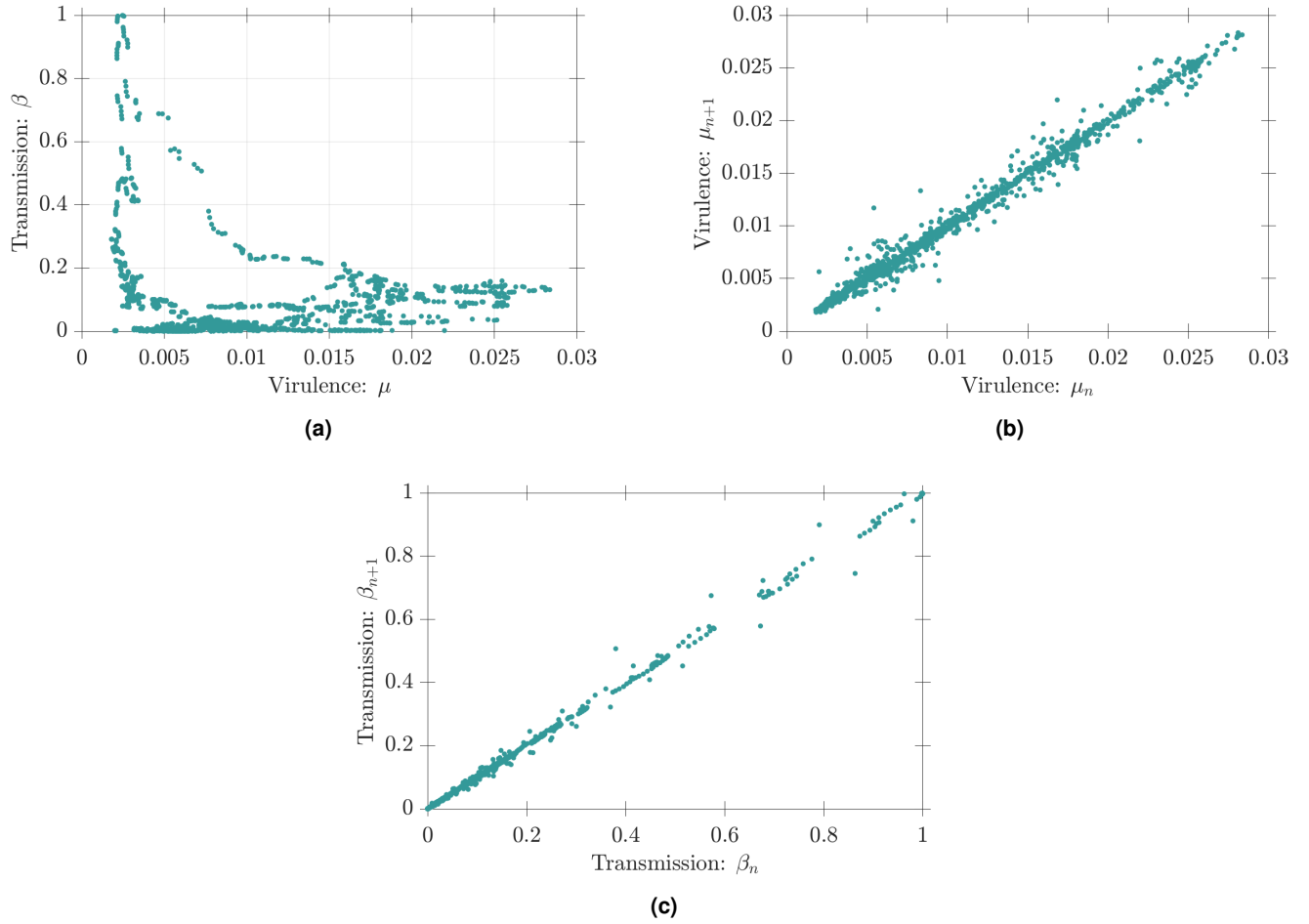


Fig. S3. Geometric investigation of SARS-CoV-2 trait dynamics for Europe. One-step relationships show that both virulence and transmission are largely self-predictive. The European data are daily observations from Our World in Data [1, 2] covering a period from September 1st, 2020, to August 24, 2025. (a) shows the joint phase space of virulence μ and transmission β . (b) shows μ_{n+1} plotted against μ_n , and (c) shows β_{n+1} plotted against β_n . As with the USA data, the European transmission series does not display the three-branch pattern reported for global transmission in the main text section 3.2.1 Figure 4c. This similarity points to a reduced role for additional causal drivers of transmission at these regional scales.

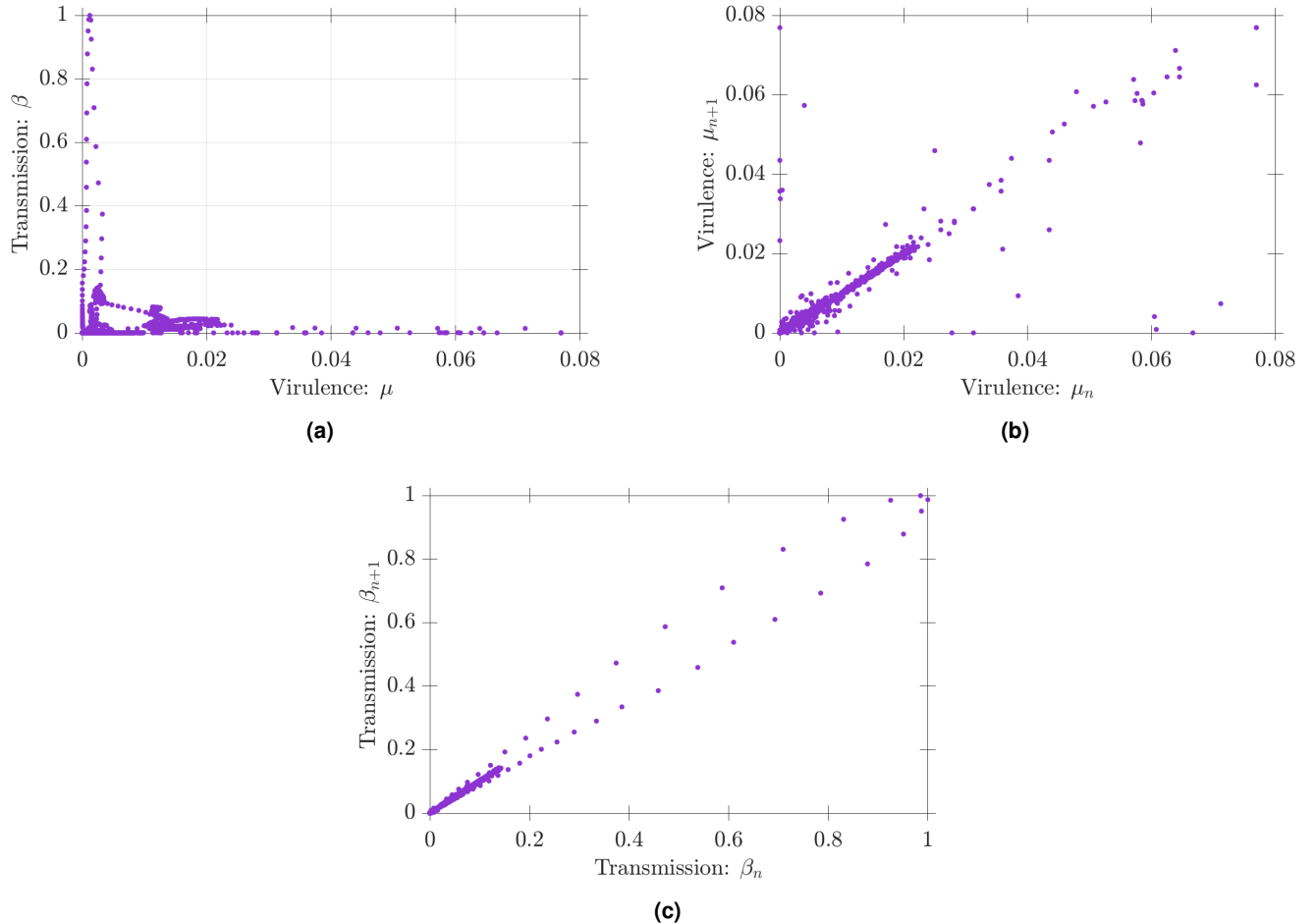


Fig. S4. Geometric investigation of SARS-CoV-2 trait dynamics for Asia. One-step relationships indicate that virulence and transmission are largely self-predictive. The data are daily observations from Our World in Data [1, 2] covering a period from September 1st, 2020, to August 24, 2025. (a) shows the joint phase space of μ and β . (b) shows μ_{n+1} versus μ_n , and (c) shows β_{n+1} versus β_n . Relative to the USA and Europe, the Asian series exhibits a modest increase in dispersion in the one-step relationships, particularly at higher values of transmission. This pattern may reflect the influence of additional causal drivers in this region.

Across regions, the virulence series exhibits consistently low correlation dimension. Estimates of $D_2(\mu_n)$ are close to unity, and the increase in $D_2([\mu_n, \mu_{n+1}])$ is modest, which indicates strong short-term predictability and a low-dimensional geometric structure. This behavior is visually reflected in the tight one-dimensional manifolds observed in the corresponding scatter plots. In contrast, the transmission series display more variable D_2 values (across regions), which suggests more complex underlying dynamics. Geometric information flow further clarifies the asymmetry between virulence and transmission. At both global and regional scales, the information flow from transmission to virulence remains weak. The corresponding $GeoC_{\beta \rightarrow \mu}$ values are small and show limited regional variation. By contrast, the flow from virulence to transmission is more pronounced at the global level and in Asia, indicating that contemporaneous virulence contains additional predictive information for subsequent transmission in those settings. The USA and Europe exhibit smaller $GeoC_{\mu \rightarrow \beta}$ values, consistent with a weaker influence of virulence on transmission.

The regional scatter plots are consistent with these quantitative findings. The USA and Europe show compact one-step relationships for virulence and comparatively limited transmission dispersion. The Asian series shows dispersion in the one-step transmission relationships, consistent with the larger estimated $GeoC_{\mu \rightarrow \beta}$ for this region. These regional patterns should be interpreted cautiously, given differences in epidemic timing, reporting practices, and the potential presence of unobserved co-variates.

S6 Supplementary notes and figures on the LETR study

S6.1 Study limitations

Despite its potential, the LETR framework has several limitations and opportunities for future development. Robust Granger-based inference requires sufficiently long and approximately stationary time series, so methodological advances for short or irregular datasets and techniques to mitigate unobserved confounding are required. Accurate causal modeling depends on distinguishing direct from indirect drivers (as illustrated in myxomatosis example), which motivates integrating tools for detecting mediated influences such as causation entropy [4]. Extending LETR to include genetic drivers will demand adaptation to high-dimensional genomic data and related extensions of Granger causality [5]. Natural systems may be stochastic due to demographic and environmental noise; incorporating stochastic transfer operators and relevant causality metrics is essential [6]. And LETR may be of use in controlled laboratory settings or in experimental evolution, where the method can more carefully hone in on causal relationships in evolving populations.

S6.2 Supplementary Figures

S6.2.1 Causal model for Granger style predictor testing

The supplementary Figure S5 presents a schematic of the nested model comparison employed in this study. The null model predicts the focal trait solely from its own lagged value, $\mu_{n+1} = f(\mu_n)$. The alternative model augments this by conditioning on a candidate predictor y_n and evaluates whether its inclusion improves one-step forecasts of μ . In practice, this test is implemented using information gain measures that quantify the predictive improvement attributable to y_n . Illustrative biological examples of such candidate predictors include transmission rate, host immune status, population density, treatment exposure, and environmental co-variates. It is important to emphasize that a positive Granger style result indicates predictive utility rather than definitive mechanistic causation. Inference may be influenced by confounding factors, unobserved drivers, measurement error, or limited temporal resolution.

S6.2.2 Pathogen passage schematics and ensemble distributions

Figure S6 depicts a single infection event in which a pathogen of generation n with traits μ_n and β_n enters a host and exits as generation $n + 1$ with updated traits μ_{n+1} and β_{n+1} . This diagram highlights that observed changes between successive records may arise during host passage through mutation, selection, transmission bottlenecks and host specific ecological effects. Figure S7 adopts an ensemble perspective and shows how

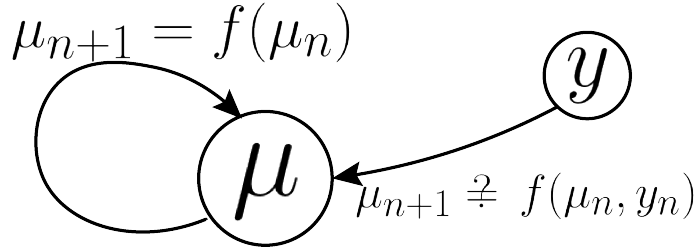


Fig. S5. Diagram of the causal model used to test Granger style predictors of a focal trait. The focal trait is denoted by μ and observations are indexed by generation n . The baseline hypothesis is that the next-generation value μ_{n+1} depends only on the previous value μ_n , written $\mu_{n+1} = f(\mu_n)$. The alternative hypothesis is that a measured variable y at the previous generation improves one step forecasts of the focal trait, written $\mu_{n+1} \neq f(\mu_n, y_n)$. In practice we test whether including y_n reduces out of sample forecast error and increases predictive information for μ . Example candidate variables y are transmission rate, host immune status, population density, treatment exposure, and environmental co-variates. A positive result should be interpreted as evidence that y carries predictive information that may reflect a causal influence under the Granger philosophy.



Fig. S6. Schematic showing a single n^{th} generation pathogen entering a host and the resulting $(n+1)^{\text{th}}$ generation pathogen exiting the host. The pathogen in generation n is characterized by virulence μ_n and transmission rate β_n . After passing through the host the pathogen in generation $(n+1)$ is characterized by updated values μ_{n+1} and β_{n+1} due to mutation, immune response, transmission bottlenecks or other within-host processes. The figure emphasizes that changes between consecutive observations may reflect both evolutionary change during host passage and host-specific effects. In time series that lack a clear generational label one unit of time can be interpreted as a generation with index n .

repeated passages across many hosts reshape the population level distribution of a focal trait. Together, these separate figures clarify the link between within host processes and population level evolution and motivate the focus on one step transition densities and invariant densities under a discrete update map. For empirical time series that lack an explicit generational label, one unit of observation may be interpreted as a generation indexed by n .

S6.2.3 Simulated time series data synthetic example and causal model

Figure S8 display the simulated time series used throughout this study. The generating maps employed in these simulations are

$$\mu_{n+1} = a \mu_n (1 - \mu_n), \quad \beta_{n+1} = 1.5 \operatorname{sech}^2(\mu_n + \beta_n),$$

with the parameter a chosen near four so that the μ update operates in the chaotic regime originally popularized in ecological applications by May [7]. The β update implements a bounded response function of μ_n and β_n so that transmission remains within a biologically plausible range. These deterministic rules were chosen to produce irregular looking trajectories for pedagogical purposes while preserving interpretable links between virulence and transmission.

In Figure S9, we present the inferred causal model derived from the simulated dataset. The figure illustrates the asymmetric relationship between virulence (μ_n) and transmission (β_{n+1}), showing that past virulence substantially improves the prediction of future transmission, whereas the reverse effect is negligible. These relationships are quantitatively supported by the geometric causal measures reported in the main text, with $GeoC_{\mu \rightarrow \beta} \approx 0.67$ and $GeoC_{\beta \rightarrow \mu} \approx 2 \times 10^{-5}$. The dominant directional link from virulence to transmission reflects the deterministic generating maps employed in the simulation, specifically $\beta_{n+1} = 1.5 \operatorname{sech}^2(\mu_n + \beta_n)$. This model illustrates

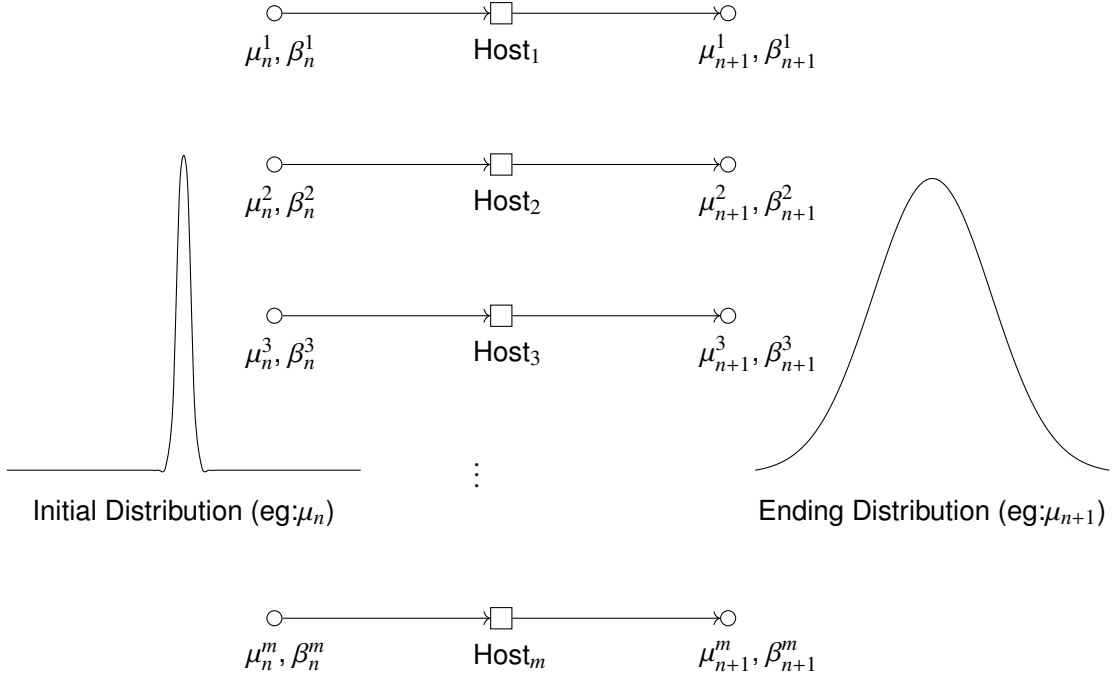


Fig. S7. Schematic representation of pathogen passage across hosts. Pathogens from generation n enter hosts carrying trait values (for example, transmission rate β or virulence μ). After undergoing within-host processes such as mutation and ecological interactions, they exit the hosts as pathogens of generation $n + 1$ with potentially altered traits. Illustrated distributions show how the values of a trait may shift from entry (generation n) to exit (generation $n + 1$).

how LETR captures mechanistic assumptions embedded in simulated data and provides a robust framework for investigating causal relationships in experimental or observational biological systems.

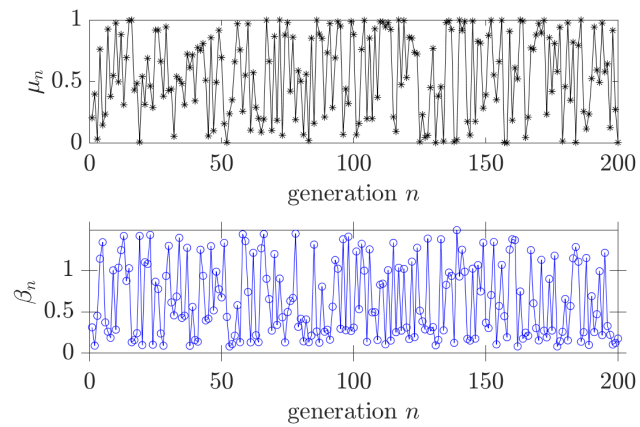


Fig. S8. Simulated time series of virulence μ_n and transmission β_n across 200 generations. The trajectories appear noisy but were generated by deterministic update rules chosen to mimic mechanistic links between virulence and transmission, following the spirit of Dwyer et al. [8]. The generating map used in the simulation is $\mu_{n+1} = a\mu_n(1 - \mu_n)$, $\beta_{n+1} = 1.5 \operatorname{sech}^2(\mu_n + \beta_n)$. The μ update is the logistic map in its chaotic regime ($a \approx 4$) and can produce complex, irregular trajectories even in the absence of external noise. The β update couples transmission to both the current virulence level and the current transmission level through a nonlinear bell-shaped bounded function, producing dependent fluctuations in transmission. These rules reproduce features seen in empirical pathogen data such as irregular trajectories, non-Gaussian trait distributions, and temporal predictability of virulence that can influence transmission.

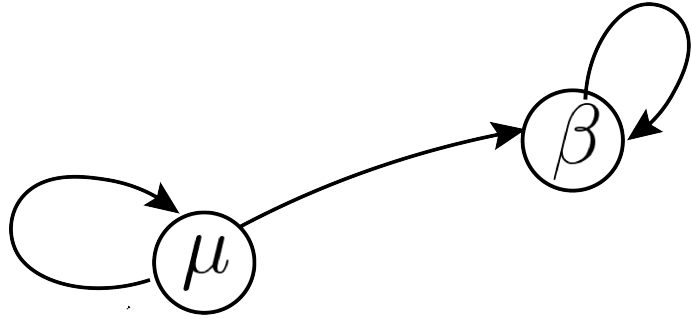


Fig. S9. Causal model summarizing the inferred relationships from the simulated dataset and supporting empirical evidence. The analysis reveals an asymmetric relationship in which past virulence (μ_n) substantially improves the prediction of future transmission (β_{n+1}), whereas the reverse effect is weak. This conclusion is quantitatively supported by the geometric causal inference measures reported in the main text (e.g., $GeoC_{\mu \rightarrow \beta} \approx 0.46$ and $GeoC_{\beta \rightarrow \mu} \approx 0.02$ in these simulations). The dominant directional link from virulence to transmission reflects the mechanistic assumptions embedded in the simulation. The generating map employed in this simulation was $\mu_{n+1} = 4\mu_n(1 - \mu_n)$, $\beta_{n+1} = 1.5 \operatorname{sech}^2(\mu_n + \beta_n)$, which capture the deterministic update rules underlying the observed dynamics. This framework can be extended to experimental or observational data to investigate causal relationships in real biological systems.

S7 Dynamics of virulence as a logistic map

In epidemiology, the case mortality rate is often used as a proxy for virulence [8]. Analogous to how the number of infected cases over time can be modeled using a logistic map [9], the case mortality rate can likewise be conceptualized as evolving according to a logistic map. This idea can be further supported through data-driven analysis. Here, we use historical real-world data on *poliomyelitis* to demonstrate that its virulence dynamics follow a logistic map. Furthermore, after investigating the poliomyelitis data we did not identify any additional causal variables. Hence we now focus exclusively on virulence as the pathogen's trait of interest, assuming no influence from transmission or other parameters on its dynamics. We further assume that virulence evolves across generations according to the logistic map with hyperparameter $0 < a \leq 4$.

Equation (12) illustrates the logistic map relationship between the n^{th} and $(n+1)^{\text{th}}$ generations of the pathogen's virulence value.

$$\mu_{n+1} = a\mu_n(1 - \mu_n). \quad (12)$$

Depending on the parameter value a , the map can demonstrate a range of behaviors, from stable fixed points to periodic orbits and chaotic dynamics. It is particularly notable for undergoing period doubling bifurcations as a increases. The chaotic behavior of the map, especially when $a = 4$ [10], is of special interest due to its relevance in practical scenarios.

S7.1 Chaos in the logistic map and long-term trait distributions

To offer a concise overview of chaotic behavior, we summarize Erik Boltt's (1997) [11] explanation. People often ask, "What is chaos good for?" This question underscores the intriguing nature of chaos [11, 12, 13]. Although chaos effectively characterizes the complexity of the world around us, its importance reaches beyond mere description. Chaos can serve as a powerful model for understanding our environment and, moreover, can be controlled and harnessed [11]. The term "chaos" is often misunderstood due to the disparity between its common English usage and its mathematical definition. In everyday language, chaos is typically associated with "extreme disorder or confusion" [14]. In contrast, the mathematical concept of chaos suggests that what appears to be random behavior may arise from an underlying deterministic and structured process. According to the well-accepted definition by Devaney [15], a one-dimensional map f of the form $x_{n+1} = f(x_n)$ is chaotic if it displays sensitive dependence on initial conditions, exhibits topological transitivity (equivalent to the existence of a dense orbit), and contains an infinite number of periodic orbits [11, 16].

The surprising insight of chaos theory is that data that appear to be randomly generated, such as the time series presented in Figure S10, are not necessarily random [11]. Therefore, the logistic map with $a = 4$ is

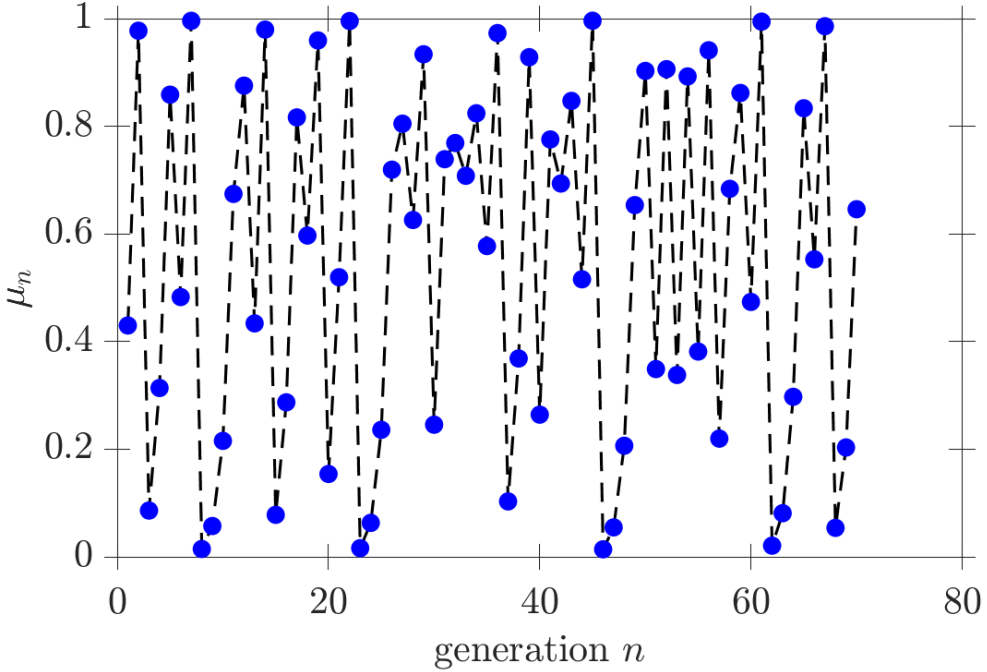


Fig. S10. Chaotic variation in a pathogen trait generated by a simple deterministic model. The time series shows the trajectory of a hypothetical focal trait (μ) across successive pathogen generations. Although the pattern appears noisy, it is generated by the logistic map, a discrete nonlinear recurrence relation popularized by the biologist Robert May in a landmark 1976 *Nature* paper[7], demonstrating how simple deterministic rules can produce complex, irregular dynamics. This example illustrates how pathogen traits (μ) may appear to fluctuate stochastically without any external randomness, reflecting deterministic ecological and evolutionary feedbacks.

employed in this study to model virulence, demonstrating the systems chaotic behavior and enabling detailed investigation of seemingly random data. Utilizing this chaotic map, we illustrate the evolution of ensembles (densities) of initial conditions under the dynamical system. As discussed in the methods section, the analysis of ensemble evolution can effectively be concluded using the Frobenius Perron operator theory. This theoretical framework is broadly applicable, accommodating various deterministic or random maps beyond the logistic map example. Readers can explore any deterministic or random map for discussions on transfer operator theory or ensemble evolution.

The logistic map with $a = 4$ is renowned for its unique absolutely continuous invariant density function [17, 18, 19] (see Figure S11a), represented by

$$\rho(\mu) = \frac{1}{\pi \sqrt{\mu(1-\mu)}}. \quad (13)$$

This closed-form expression of the invariant density for the logistic map enables detailed analysis. Regardless of the initial distribution of the variable, the long-term distribution converges to this invariant density (Equation (13)), as shown in Figure S11b. As observed in Figure S11, the density is higher around 0 and 1 than at other values. In the context of virulence, this implies that, regardless of the initial distribution of virulence values in the pathogen population, the long-term trend is to see the majority of the population leaning towards either the lowest virulence (zero) or the highest virulence (one), with a significantly lower density in the intermediate range.

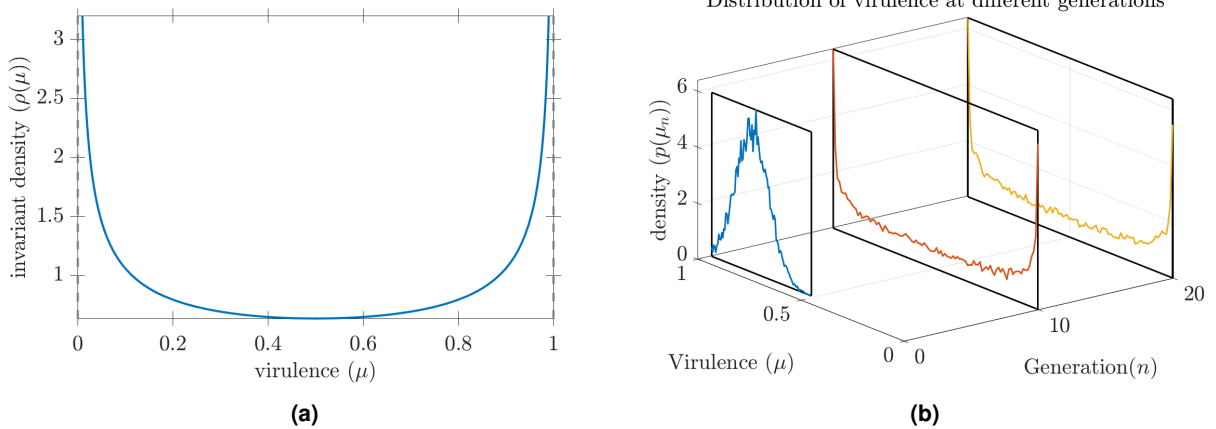


Fig. S11. Long term dynamics of pathogen virulence modeled by the logistic map. (a) The invariant density of the logistic map with $a = 4$ is given by $\rho(\mu) = \frac{1}{\pi\sqrt{\mu(1-\mu)}}$, indicating that trait values near 0 and 1 are more frequently visited after many generations. (b) The evolution of the trait distribution over successive generations demonstrates convergence to this invariant density. This pattern suggests that, in the context of virulence, pathogen populations are more likely to evolve towards either very low or very high virulence in the long-term, with a significantly lower population density in the intermediate range. This pattern is reminiscent of certain ecological and evolutionary scenarios in host–parasite systems, where selective pressures may favor either very low or very high virulence strategies over intermediate values [20, 21]. This illustrates how simple deterministic models can capture complex evolutionary patterns in pathogen traits.

Supporting Information References

- [1] Edouard Mathieu, Hannah Ritchie, Lucas Rodés-Guirao, Cameron Appel, Daniel Gavrilov, Charlie Giattino, Joe Hasell, Bobbie Macdonald, Saloni Dattani, Diana Beltekian, Esteban Ortiz-Ospina, and Max Roser. *Mortality Risk of COVID-19*. Our World in Data. Online: <https://ourworldindata.org/mortality-risk-covid>. 2020.
- [2] Edouard Mathieu, Hannah Ritchie, Lucas Rodés-Guirao, Cameron Appel, Daniel Gavrilov, Charlie Giattino, Joe Hasell, Bobbie Macdonald, Saloni Dattani, Diana Beltekian, Esteban Ortiz-Ospina, and Max Roser. *COVID-19 Cases*. Our World in Data. Online: <https://ourworldindata.org/covid-cases>. 2020.
- [3] The MathWorks, Inc. *correlationDimension: Measure of chaotic signal complexity*. <https://www.mathworks.com/help/predmaint/ref/correlationdimension.html>. 2025.
- [4] Jie Sun and Erik M Boltt. "Causation entropy identifies indirect influences, dominance of neighbors and anticipatory couplings". In: *Physica D: Nonlinear Phenomena* 267 (2014), pp. 49–57.
- [5] Shuixia Guo, Christophe Ladroue, and Jianfeng Feng. "Granger causality: theory and applications". In: *Frontiers in computational and systems biology*. Springer, 2010, pp. 83–111.
- [6] Demetris Koutsoyiannis, Christian Onof, Antonis Christofides, and Zbigniew W Kundzewicz. "Revisiting causality using stochastics: 1. Theory". In: *Proceedings of The Royal Society A* 478.2261 (2022), p. 20210835.
- [7] Robert M May. "Simple mathematical models with very complicated dynamics". In: *Nature* 261.5560 (1976), pp. 459–467.
- [8] Greg Dwyer, Simon A Levin, and Linda Buttel. "A simulation model of the population dynamics and evolution of myxomatosis". In: *Ecological monographs* 60.4 (1990), pp. 423–447.
- [9] George Sugihara and Robert M May. "Nonlinear forecasting as a way of distinguishing chaos from measurement error in time series". In: *Nature* 344.6268 (1990), pp. 734–741.
- [10] R Devaney. "An Introduction to Chaotic Dynamical Systems". In: *An Introduction to Chaotic Dynamical Systems* (1989).
- [11] Erik M Boltt. "Controlling the chaotic logistic map". In: *Problems, Resources, and Issues in Mathematics Undergraduate Studies* 7.1 (1997), pp. 1–17.
- [12] Martin C Gutzwiller. "Chaos in classical and quantum mechanics". In: vol. 1. Springer Science & Business Media, 2013. Chap. 1.
- [13] Linda B Smith and Esther Ed Thelen. "A dynamic systems approach to development: Applications." In: *This book grew out of a workshop," Dynamic Systems in Development," held for the Society for Research in Child Development in Kansas City, KS, Apr 1989*. The MIT Press. 1993.
- [14] "Oxford American Dictionary". In: *New York, NY: Avon Books* (1986).
- [15] Robert Devaney. *An introduction to chaotic dynamical systems*. CRC press, 2018.
- [16] Erik M Boltt and James D Meiss. "Targeting chaotic orbits to the Moon through recurrence". In: *Physics Letters A* 204.5-6 (1995), pp. 373–378.
- [17] Andrzej Lasota and Michael C Mackey. *Chaos, Fractals, and Noise: Stochastic Aspects of Dynamics*. Vol. 97. Springer Science & Business Media, 1998.
- [18] Erik M Boltt. "Controlling chaos and the inverse Frobenius–Perron problem: global stabilization of arbitrary invariant measures". In: *International Journal of Bifurcation and Chaos* 10.05 (2000), pp. 1033–1050.
- [19] Sudam Surasinghe, Jeremie Fish, and Erik M Boltt. "Learning transfer operators by kernel density estimation". In: *Chaos: An Interdisciplinary Journal of Nonlinear Science* 34.2 (2024).
- [20] M Van Baalen. "Coevolution of recovery ability and virulence". In: *Proceedings of the Royal Society of London. Series B: Biological Sciences* 265.1393 (1998), pp. 317–325.

[21] Jessica L Hite and Clayton E Cressler. "Resource-driven changes to host population stability alter the evolution of virulence and transmission". In: *Philosophical Transactions of the Royal Society B: Biological Sciences* 373.1745 (2018), p. 20170087.